Available online at www.sciencedirect.com
ScienceDirect
Geochimica et Cosmochimica Acta 70 (2006) 5469–5487
Geochimica
www.elsevier.com/locate/gca

Molecular characterization of uranium(VI) sorption complexes on iron(III)-rich acid mine water colloids

Kai-Uwe Ulrich [a,*], André Rossberg [a,b], Harald Foerstendorf [a], Harald Zänker [a], Andreas C. Scheinost [a,b]

[a] *Institute of Radiochemistry, FZ Rossendorf e.V., P.O. Box 510119, D-01314 Dresden, Germany*
[b] *Rossendorf Beamline at ESRF, B.P. 220, F-38043 Grenoble, France*

Received 7 November 2005; accepted in revised form 21 August 2006

Abstract

A mixing of metal-loaded acid mine drainage with shallow groundwater or surface waters usually initiates oxidation and/or hydrolysis of dissolved metals such as iron (Fe) and aluminum (Al). Colloidal particles may appear and agglomerate with increasing pH. Likewise chemical conditions may occur while flooding abandoned uranium mines. Here, the risk assessment of hazards requires reliable knowledge on the mobility of uranium (U). A flooding process was simulated at mesocosm scale by mixing U-contaminated acid mine water with near-neutral groundwater under oxic conditions. The mechanism of U-uptake by fresh precipitates and the molecular structure of U bonding were determined to estimate the mobility of U(VI). Analytical and spectroscopic methods such as Extended X-ray Absorption Fine-Structure (EXAFS) spectroscopy at the Fe K-edge and the U L_{III}-edge, and Attenuated Total Reflectance Fourier Transform Infrared (ATR-FTIR) spectroscopy were employed. The freshly formed precipitate was identified as colloidal two-line ferrihydrite. It removed U(VI) from solution by sorption processes, while surface precipitation or structural incorporation of U was not observed. EXAFS data suggest a mononuclear inner-sphere, edge-sharing complex of U(VI) with ferrihydrite in the absence of dissolved carbonate. By employing a novel EXAFS analysis method, Monte Carlo Target Transformation Factor Analysis, we could for the first time ascertain a 3-D configuration of this sorption complex without the necessity to invoke formation of a ternary complex. The configuration suggests a slightly tilted position of the adsorbed UO_2^{2+} unit relative to the edge-sharing $Fe(O,OH)_6$ octahedra. In the presence of dissolved carbonate and at pH ~8.0, a distal carbonate O-atom at ~4.3 Å supports formation of ternary U(VI)-carbonato surface complexes. The occurrence of these complexes was also confirmed by ATR-FTIR. However, in slightly acidic conditions (pH 5–6) in equilibrium with atmospheric CO_2, the U(VI) sorption on ferrihydrite was dominated by the binary complex species $\equiv Fe(O)_2{=}UO_2$, whereas ternary U(VI)-carbonato surface complexes were of minor relevance. While sulfate and silicate were also present in the mine water, they had no detectable influence on U(VI) surface complexation. Our experiments demonstrate that U(VI) forms stable inner-sphere sorption complexes even in the presence of carbonate and at slightly alkaline pH, conditions which previously have been assumed to greatly accelerate the mobility of U(VI) in aqueous environments. Depending on the concentrations of U(VI) and carbonate, the type of surface complexes may change from binary uranyl-ferrihydrite to ternary carbonato-uranyl-ferrihydrite complexes. These different binding mechanisms are likely to influence the binding stability and retention of U(VI) at the macroscopic level.

1. Introduction

Natural weathering processes and mining activities (e.g., in situ ore leaching) contribute to mobilizing uranium (U) from its ore deposits. In Eastern Germany, about 220,000 metric tons of U were mined between 1946 and 1991, when the operations were stopped for economic and political reasons. The abandoned mines comprise a subsurface void volume greater than 10^8 m^3 which has been or can be flooded. In addition, 5×10^8 tons of radioactive mining waste were spread over 3000 piles and 20 tailings within densely populated areas (Beleites, 1992). Therefore, the prediction

* Corresponding author. Present address: Washington University, Environmental Engineering Science, Campus Box 1180, St. Louis, MO 63130, USA.
E-mail address: k.ulrich@seas.wustl.edu (K.-U. Ulrich).

0016-7037/$ - see front matter © 2006 Elsevier Inc. All rights reserved.
doi:10.1016/j.gca.2006.08.031

of potential risks associated with U migration within the aquifers and with dissemination of U-contaminated water is of high public interest. Sound predictions require reliable knowledge on the U species in both the liquid and the colloid-borne phases, and on the structure and stability of their sorption complexes.

In its hexavalent form, uranium usually exists in the environment as the uranyl dication UO_2^{2+} which can form highly soluble complexes with a variety of anionic species; including fluoride (F^-), chloride (Cl^-), carbonate (CO_3^{2-}), nitrate (NO_3^-), sulfate (SO_4^{2-}), phosphate ($H_xPO_4^{(3-x)}$), silicate ($Si(OH)_4$), and acetate (CH_3COO^-), commonly increasing the solubility of U (e.g., Langmuir, 1978). However, often sorption to mineral phases such as the hydrous oxides of Fe, Al, silicon (Si), manganese (Mn), and titanium (Ti) controls the mobility of U(VI) (Hsi and Langmuir, 1985). The sorption is dependent on pH, the activity and ratio of U(VI) and corresponding sorption sites, and the ionic composition of the liquid phase. The strongest affinity of U(VI) to hydrous ferric oxides is pH range from 5 to 8, commonly found when acid pore water from the ore deposit or acid mine drainage (AMD) mixes with non-acidic adit water, groundwater, or surface water. This water mixing may occur in the mines, especially in abandoned mines that are subject to flooding (Zänker et al., 2003), in adjacent groundwater aquifers, or in surface waters that are affected by AMD (e.g., Kimball et al., 1995). Chemical reactions such as oxidation, hydrolysis, and precipitation contribute to the formation of colloids and their agglomerates consisting mainly of Fe(III) and Al(III) oxyhydroxides and hydroxysulfates and characterized by a large surface area with many reactive sites of functional groups (Webster et al., 1998; Nordstrom and Alpers, 1999; Lee et al., 2002).

Acid mine waters usually contain high sulfate concentrations. In presence of a total uranium concentration [U_{tot}] of 0.075 mM, the dominant aqueous complexes are $UO_2SO_4^0$ and $UO_2(SO_4)_2^{2-}$ (Bernhard et al., 1998). Majzlan and Myneni (2005) attributed the dominating Fe(III) sulfate species in oxidized AMD solutions rich in SO_4^{2-} (15 mM) and Fe (10–50 mM) to hydrogen-bonded complexes. These could be present in the tentative structure of nanocrystalline schwertmannite ($Fe_{16}O_{16}(OH)_{12\text{-}9}(SO_4)_{2\text{-}3.5} \cdot nH_2O$, $n \sim 10$) that controls the Fe(III) solubility at intermediate pH ($3 < pH < 6$). Walter et al. (2003) investigated the surface complexes of U(VI) on schwertmannite in acidic (pH 4.2) solutions of Na_2SO_4 and $NaClO_4$ (each 10 mM). In contrast to the aqueous U(VI) sulfato complexes where the sulfate ion is bidentately coordinated to U(VI) (Moll et al., 2000), the corresponding ternary surface complex $\equiv Fe(O)_2{=}UO_2(OH){=}SO_4$ (Fig. 1A) could not be verified by U L_{III}-edge EXAFS spectroscopy. However, previous EXAFS results support the formation of binuclear, bidentate and mononuclear, monodentate inner-sphere surface complexes of U(VI) with structural sulfate of schwertmannite (Walter et al., 2003).

Silicate ions are also expected to influence the surface complexation of U(VI), since SiO_4^{4-} ligands are known to influence the hydrolysis of Fe(III) (Doelsch et al., 2003). The UO_2^{2+} cation has a strong affinity to amorphous silica gel between pH 4 and 7 (Dent et al., 1992; Moll et al., 1998) and may form an inner-sphere, mononuclear, edge-sharing complex with silicate tetrahedra (Fig. 1B) as was proposed from U L_{III}-edge EXAFS spectroscopy (Reich et al., 1998). Moyes et al. (2000) explain the adsorption of U(VI) onto muscovite ($KAl_2(OH)_2AlSi_3O_{10}$) by surface precipitation, with the first layer of uranium atoms being similarly coordinated with silicate tetrahedra. In a comprehensive study on the mechanism and structure of U sorption on natural Si-/Al- and Fe-rich gels in a granitic U deposit, Allard et al. (1999) proposed a two step U-uptake process, the initial complexation of U(VI) by Si or Al, followed by trapping of these complexes within hydrous ferric oxides during precipitation.

Carbonate is another ubiquitous component of groundwater and non-acidified surface waters that forms strong aqueous complexes with UO_2^{2+} (Grenthe et al., 1992; de Jong et al., 2005). Aqueous species such as $Ca_2UO_2(CO_3)_{3(aq)}$ (Bernhard et al., 1996) and $UO_2(CO_3)_3^{4-}$ prevent the adsorption of U(VI) onto mineral surfaces at $pH > 7$ (Wazne et al., 2003). However, dissolved carbonate may also form strong surface complexes on ferric hydroxides (Van Geen et al., 1994; Su and Suarez, 1997; Bargar et al., 2005). Hence, the surface complex species which result from competitive interaction between dissolved carbonate and U(VI) are of special interest. Bargar et al. (1999, 2000) concluded from ATR-FTIR and EXAFS spectra, and electrophoretic mobility measurements that monomeric hematite-U(VI)-carbonato complexes with bidentate coordination of carbonate to the equatorial oxygen atoms of UO_2^{2+} dominate at [U_{tot}] $\leqslant$ 0.012 mM and pH 4.5–6.5 (Fig. 1C), and proposed dimeric ternary complexes at pH 8.5. Consequently, the authors postulate that Fe-oxide-U(VI)-carbonato complexes are important transport-limiting species in oxic aquifers over a wide pH range.

EXAFS spectroscopy is not as sensitive as ATR-FTIR to identify molecular interactions of carbonate ligands. Additional information on the system is needed to uniquely assign an atom type to a signal. A typical example is the interpretation of the peak at about 2.4 Å (uncorrected for phase shifting) in the Fourier transform (FT) of U L_{III}-edge EXAFS spectra of U(VI) sorption complexes. This peak has been assigned to carbon (Bargar et al., 2000), to chlorine (Redden et al., 2001), and may refer to nitrogen as well (Thompson et al., 1997). Despite the absence of nitrate and great care to exclude carbonate, this peak also appeared in spectra of U(VI) sorbed schwertmannite and goethite (α-FeOOH) at a pH as low as 4.2 (Walter et al., 2003), which would further reduce the solubility of carbonate if present. The contribution of chlorine is unlikely

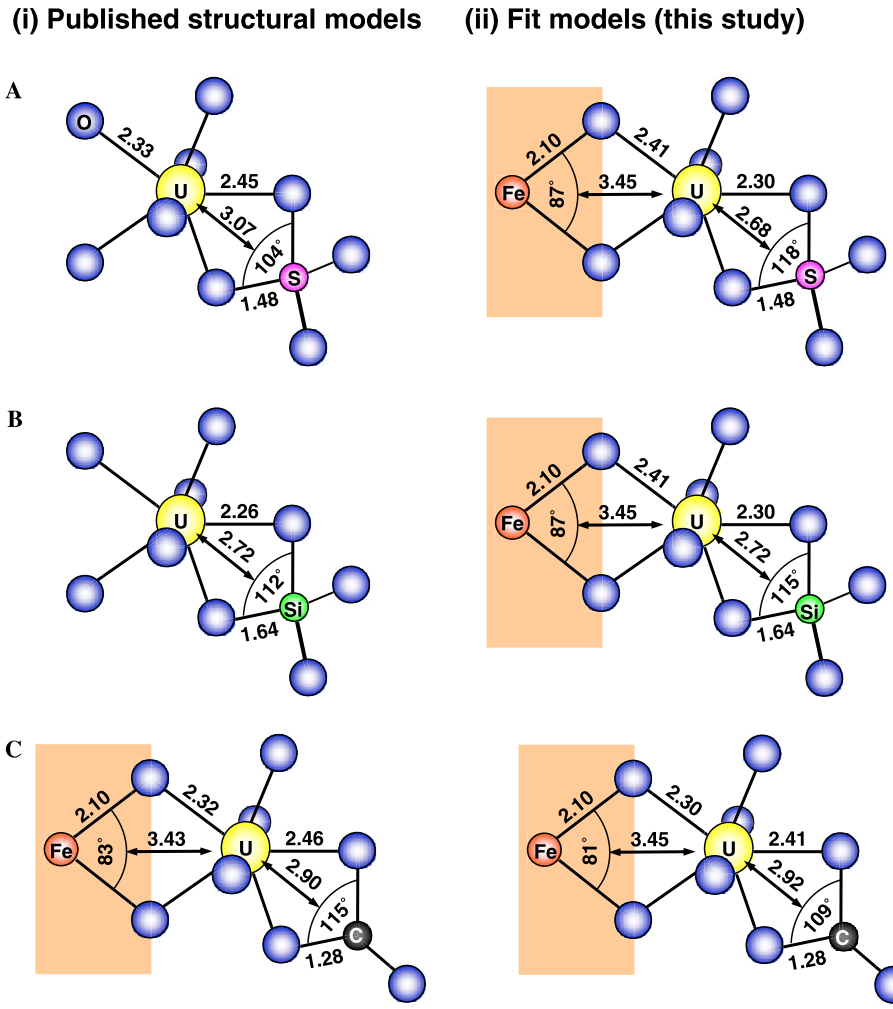

Fig. 1. Ball-and-stick representation of (i) published structural models and (ii) fit models of the present study with bidentate coordination of uranyl and sulfate (A), silicate (B), and carbonate (C). Blue (dark grey) balls are oxygen atoms, hydrogen atoms are omitted for clarity. The Fe oxyhydroxide surface is depicted by the shaded area; for clarity only the two Fe—O bonds pointing towards the surface are shown, representing an octahedral surface edge. The numbers are calculated angles (°) and interatomic distances (Å). Coordination of U(VI) to (A) sulfate adapted from the solid $UO_2SO_4 \cdot 2CH_3CON(CH_3)_2$ (Blatov et al., 1990), (B) silicate as proposed by Reich et al. (1998), and (C) carbonate according to Bargar et al. (2000). (For interpretation of the references to color in this figure legend, the reader is referred to the web version of this paper.)

because the chosen perchlorate background concentration was much below the level needed to form inner-sphere complexes with uranyl (Sémon et al., 2001). Hence within these systems the FT peak at 2.4 Å is more likely attributed to oxygen than to carbon, nitrogen, or chlorine.

The present study focuses on the local structure of colloid-borne U(VI) originating from uranium mines in the process of being flooded. We simulated a mine flooding scenario in the laboratory to obtain sufficient colloidal matter for spectroscopic and other analyses. Since the composition of mine water is often very complex, we tested the influence on U sorption structures of some of the major ligands by a set of simplified sorption experiments under controlled conditions, and applied EXAFS and ATR-FTIR spectroscopies to elucidate the surface complex structures at the molecular level.

2. Experimental and analytical methods

2.1. Mine flooding simulation

In situ leaching of uranium by sulfuric acid has been applied at the Königstein uranium mine (Saxony, Germany) between 1967 and 1991, thereby contaminating 5.5×10^7 metric tons of sandstone. Flooding of the mine has been monitored since 1992. A mesocosm experiment was designed to simulate the scenario of gradually flooding up to the stage where potentially contaminated water penetrates groundwater aquifers or surface water. Two types of water samples were taken from the mine: (i) acid mine water from an early stage of the mine flooding process, contaminated by uranium and other heavy metals, and (ii) near-neutral, suboxic shallow groundwater from an aquifer above the mine (Table 1). These two waters were

Table 1
Analysis of acid mine water from the Königstein uranium mine and of groundwater from an overlying aquifer

Parameter	Mine water	Groundwater
pH	2.85	6.50
E_H	480	290
EC	2.09	0.255
[O_2]	0.4	6.6
[TIC]	10.5	15.1
[TOC]	1.3	0.33
[SO_4^{2-}]	1260	64.8
[Al]	39.2	0.50
[Ca]	122	35.5
[Fe(II)]	192	2.4
[Fe(III)]	84.0	0.8
[K]	4.0	1.6
[Mg]	17.2	3.1
[Mn]	12.4	0.012
[Na]	25.2	4.9
[Si]	5.7	1.7
[U]	16.3	0.005
[Zn]	12.2	0.12

E_H in mV, electrical conductivity (EC) in mS cm^{-1}, concentrations in mg L^{-1}. TIC, total inorganic carbon; TOC, total organic carbon.

mixed in a 120 L vessel in the laboratory by stepwise adding within five days groundwater aliquots of 10–20 L to the initial volume of floodwater (5–6 L). Oxygenation by small gas bubbles provided turbulence and accelerated the oxidation of Fe(II). Total iron (Fe_{tot}) was analyzed by AAS-GF (ZEEnit 60, Analytik Jena), and Fe^{2+} spectrophotometrically by the 1,10-phenanthroline method (DIN 38406-E1-1). Electrodes (WTW, Weilheim) were used to record pH and electrical conductivity (EC) over time. Three experiments with final pH ranges of 5.0–5.5, 5.5–6.0, and 4.5–5.0 were carried out to study the corresponding precipitates designated M1, M2, and M3.

After 4–5 days the partially agglomerated colloids were characterized in their original suspension by photon correlation spectroscopy (Brookhaven BI-90), and by laser Doppler electrophoresis (Malvern Zetasizer 3000HSA). Small aliquots of the suspension were filtered through rinsed Nucleopore® filter membranes with a pore size of either 50 nm or 1 μm, and the membranes were repeatedly washed with de-ionized MilliQ® water before being dried in a desiccator. The particles deposited on the filter membrane were visualized by Scanning Electron Microscopy (SEM) and analyzed by energy-dispersive X-ray spectroscopy, after sputtering the surface with a thin carbon layer. Tangential flow 30 kD ultra-filtration (Amicon hollow fiber cartridge type H5P30-43) followed by ultra-centrifugation (Beckman Coulter XL-look, 285,000*g*; 30 min) was used to concentrate the suspended precipitate to a wet paste. A fraction of the paste was loaded into two polyethylene vials, one of which designed for EXAFS measurement at room temperature, the other for use on a cryostat sample holder (see Section 2.3). The latter sample was immediately shock-frozen in liquid nitrogen and stored therein until running the EXAFS measurement to avoid aging of the sample. The EXAFS sample spectra of both preparation techniques were compared for structural changes at the molecular scale. After air-drying and pulverization of the remaining paste aliquot, Cu Kα X-ray powder diffraction (Bruker D8 Advance) and Mössbauer spectroscopy were applied at room temperature. The major elements of the precipitate were analyzed by ICP-MS (ELAN 6000, Perkin Elmer), AAS-F (4100, Perkin Elmer), and AAS-GF (ZEEnit 60, Analytik Jena), after microwave supported acid digestion.

2.2. Sorption experiments

A first series of batch experiments (S1–S7) aimed at studying the influence of environmentally relevant concentrations of sulfate and silicate on the uptake and complex structure of U(VI) on ferrihydrite (nominal formula $Fe_5HO_8 \cdot 4H_2O$). Solutions of 1 mM $Fe(NO_3)_3 \cdot 9H_2O$, 15 mM $NaNO_3$ (background electrolyte), and 0.012 mM $UO_2(NO_3)_2$ with either sulfate or silicate or both were adjusted to pH 5.5 by dropwise adding 1 M or 0.1 M NaOH solution under vigorous stirring at atmospheric pCO_2 of 35.5 Pa (Table 2). The pH was re-adjusted after 6, 12, and 24 h. After 24 h of equilibration, the aggregated colloids were allowed to settle for 65–70 h and then (at an age of ~95 h) concentrated to wet pastes by ultra-centrifugation (285,000 *g*; 30 min). The pastes were transferred into polyethylene vials and stored in liquid N_2 to avoid aging alterations before the EXAFS measurement. Further ferrihydrite precipitates were prepared likewise, but in a N_2 flushed glovebox ($pCO_2 < 0.2$ Pa) with 0.05 mM $UO_2(NO_3)_2$ (S8) and without UO_2^{2+} (S9).

The total NO_3^- concentrations were held below 0.02 M to avoid ternary complex formation with the adsorbed UO_2^{2+}. According to reported EXAFS data, the ions of a 0.1 M $UO_2(NO_3)_2$ solution fully dissociate and form the pentahydrated $[UO_2(H_2O)_5]^{2+}$ species (Sémon et al., 2001). To cross-check this, we prepared additional samples using the salts of chloride or perchlorate instead of nitrate, because these ions are excluded from complex formation with UO_2^{2+} at the given electrolyte concentration (Sémon et al., 2001; Hennig et al., 2005). The EXAFS data revealed no spectral difference to the samples prepared with nitrate background electrolyte, rendering nitrate complexation to the adsorbed U(VI) in our samples unlikely.

A second series of batch experiments was performed to study the influence of pCO_2 and dissolved carbonate on the U(VI) sorption species. Ferrihydrite was prepared from solutions of 1 mM $FeCl_3 \cdot 6H_2O$, 15 mM NaCl (background electrolyte), and varying concentrations of UO_2Cl_2 ([U_{tot}] of 0, 6, 12, 30, 50, 60, 75, 100 μM) added at atmospheric pCO_2 of 35.5 Pa or in a CO_2-free atmosphere ($pCO_2 < 0.2$ Pa, [U_{tot}] of 0, 12, 50, 100 μM). Two different final pH levels, pH 5.5 and pH 8.0, were adjusted at an accuracy of ±0.05 pH units by adding NaOH solution. The suspended precipitates at an age of ~95 h were concentrated to wet pastes as described above and immediately

Table 2
Key parameters of sorption experiments carried out with [Fe_{tot}] of 1 mM

Sample	pCO_2 (Pa)	Initial [UO_2^{2+}] (mM)	Final pH	U uptake (%)	Colloidal fraction (%) relative to the initial concentration of added ions
S1	35.5	0.012	5.5	98.2	7.6% of 1.2 mM SO_4^{2-}
S2	35.5	0.012	5.5	95.6	3.5% of 4.8 mM SO_4^{2-}
S3	35.5	0.012	5.5	99.3	66.5% of 0.075 mM $Si(OH)_4$
S4	35.5	0.012	5.5	98.9	63.2% of 0.3 mM $Si(OH)_4$
S5	35.5	0.012	5.5	98.3	32.4% of 1.2 mM $Si(OH)_4$
S6	35.5	0.012	5.5	99.2	5.2% of 1.2 mM SO_4^{2-}, 34.2% of 1.2 mM $Si(OH)_4$
S7	35.5	0.012	5.5	96.3	4.8% of 4.8 mM SO_4^{2-}, 31.8% of 0.3 mM $Si(OH)_4$
S8	<0.2	0.050	5.5	n.a.[a]	
S9	<0.2	0	5.5	—	
S10	35.5	0.012	5.5	99.3	
S11	<0.2	0.012	5.5	99.4	
S12	35.5	0.012	8.0	98.7	Addition of 0.67 mM $NaHCO_3$
S13	<0.2	0.012	8.0	99.9	

Uranium uptake on the formed precipitates and colloidal fraction of added sulfate and silicate is based on 3 kD ultra-filtration. The solid phase had a mole ratio U/Fe = 0.0122 ± 0.0005.
[a] 'n.a.' represents 'parameter not analyzed'.

analyzed by ATR-FTIR at room temperature without further treatments. Four sub-samples of the batch series (S10–S13) were frozen in liquid N_2 prior to EXAFS analysis (Table 2).

Although generated by a typical coprecipitation approach, it was not expected that U(VI) would coprecipitate with ferrihydrite because the solubility limits of known U(VI) solids were not exceeded (Lefèvre et al., 2006). Nevertheless, U(VI) may be occluded by the precipitating ferrihydrite during this experiment analogous to the formation of 3d-metal substituted (Gerth, 1990; Schwertmann and Pfab, 1996; Manceau et al., 2000; Scheinost et al., 2001a) and U(VI) substituted oxyhydroxides (Duff et al., 2002). In contrast to typical sorption experiments, this coprecipitation approach was chosen to simulate the formation of colloids in mine waters, encompassing comparatively low concentrations of Fe and U, and avoiding drying or other alterations of the freshly precipitated ferrihydrite gel, which may change its morphology and sorption properties (Scheinost et al., 2001b).

2.3. EXAFS data collection and analysis

The measurements were carried out at the Rossendorf Beamline (BM 20) located at the European Synchrotron Radiation Facility (ESRF), Grenoble (France), using a Si(1 1 1) double crystal monochromator. Technical details of the experimental station and the beamline optics are given elsewhere (Reich et al., 2000). Iron K-edge spectra were collected in transmission mode using argon-filled ionization chambers. Uranium L_{III}-edge spectra were recorded in fluorescence mode using a solid-state 13-element germanium fluorescence detector (Canberra Corp.) with digital signal processing (XIA, Hayward, CA). Six to eight scans of each sample were collected in equidistant k-steps of 0.05 $Å^{-1}$ across the EXAFS region and then averaged to improve the signal-to-noise ratio. An Fe or Y metal foil was recorded simultaneously with the Fe K-edge and U L_{III}-edge sample measurements to calibrate the energy axis of the spectra by assigning the first inflection point at 7111.3 eV (Fe) or 17,038 eV (Y). The threshold energy, $E_{k=0}$, was defined as 7130 eV for the Fe K-edge, and as 17,185 eV for the U L_{III}-edge. A helium cryostat (Oxford) was used to cool the samples to ~30 K during the measurement to reduce thermal contributions to the Debye–Waller factors (σ^2) and to improve the detection of atoms beyond the first coordination sphere.

EXAFS data were extracted from the raw absorption spectra by standard methods including dead-time correction of the fluorescence signal, spline approximation for the atomic background, and shell fitting using the software packages EXAFSPAK (George and Pickering, 2000) or WINXAS 3.0 (Ressler, 1998). Due to increasing noise levels at higher k-range, data analysis was restricted to the k-range 2.3–14.0 $Å^{-1}$ for Fe(III) and 3.2–13.0 $Å^{-1}$ for U(VI) unless otherwise noted. The distance resolution, $\Delta R = \pi/2\Delta k$, was 0.13 and 0.16 Å for Fe(III) and U(VI), respectively. Theoretical phase and amplitude functions were calculated with the software FEFF 8.20 (Ankudinov et al., 1998) by using a hypothetical sorption complex of UO_2^{2+} on a $Fe^{III}(H_2O)_6$ octahedron of the unit cell of hematite (cf. Fig. 7D).

According to Li et al. (1995), the amplitude reduction factor, S_0^2, is approximately constant for a given absorber element in similar chemical environments. Using FEFF 8.20, we calculated S_0^2 of 0.94 ± 0.06 for a reference spectrum of uranyl pentahydrate. S_0^2 was fixed to 0.9 which is in accordance to previous EXAFS investigations (Hennig et al., 2005). This gives a maximum error in coordination number (CN) of about ±20%. The maximum error of our CN values results from the approximated S_0^2 (±20%) plus the standard deviation of CN calculated by the EXAFSPAK fitting routine. The Tables 3–5 show the fit parameters and their standard deviation given in parentheses.

Table 3
Fit parameters to the Fe K-edge EXAFS data of the simulated mine-water precipitate M2, and of the ferrihydrite reference samples S8 and S9

Sample	Shell	CN[a]	R[b] (Å)	σ^2[c] (Å^2)	ΔE_0 (eV)	χ_v^2[d]
M2	Fe—O_1	2.0(1)	1.94(1)	0.005(1)	−2.86(9)	0.20
	Fe—O_2	3.0(1)	2.07(4)	0.010(3)	#	
	Fe—Fe_1	1.01(3)	2.885(1)	0.0086(3)	#	
	Fe—Fe_2	2.6(1)	3.066(1)	#	#	
	Fe—Fe_3	0.81(5)	3.371(2)	#	#	
	Fe—Fe_4	0.70(2)	3.920(2)	#	#	
S8	Fe—O_1	3.22(6)	1.941(1)	0.0056(1)	−4.12(1)	0.10
	Fe—O_2	1.69(5)	2.065(1)	0.0042(1)	#	
	Fe—Fe_1	0.51(1)	2.960(1)	0.00406(2)	#	
	Fe—Fe_2	1.01(1)	3.071(1)	#	#	
	Fe—Fe_3	1.08(1)	3.448(1)	#	#	
	Fe—Fe_4	0.26(1)	3.992(1)	#	#	
S9	Fe—O_1	3*	1.928(1)	0.00452(1)	−4.46(1)	0.12
	Fe—O_2	2.13(1)	2.056(1)	0.00380(2)	#	
	Fe—Fe_1	0.50(1)	2.942(1)	0.00514(2)	#	
	Fe—Fe_2	1.33(1)	3.059(1)	#	#	
	Fe—Fe_3	1.51(1)	3.448(1)	#	#	
	Fe—Fe_4	0.30(1)	4.000(1)	#	#	

To reduce the number of free variables, some of them were correlated (#) or fixed (*) during the fitting. Asymptotic standard deviations are given in parentheses.
[a] Coordination number.
[b] Interatomic distance.
[c] Debye–Waller factor.
[d] Goodness-of-fit parameter according to Section 2.3., Eq. (1).

The CN of the uranyl oxygen atoms (O_{ax}) was held constant at 2. The 2-fold degenerated 4-legged multiple-scattering path U—O_{ax1}—U—O_{ax2} ($MS_{U=O}$) was included on the curve fit by constraining its effective path length and its Debye–Waller factor to twice the values of the corresponding, freely fit U—O_{ax} single-scattering path (Hudson et al., 1996). The energy shift parameter, ΔE_0, was linked for all shells.

Evaluating the quality of fits performed in k-space, the EXAFSPAK software provides the reduced chi-squared value, χ_v^2, by

$$\chi_v^2 = \sum(\chi_{exp}(k)k^3 - \chi_{theo}(k)k^3)^2/(P-F) \quad (1)$$

with k being the photoelectron wavenumber, a measure of the photoelectron wavelength (λ_e), $k = 2\pi/\lambda_e$; $\chi_{exp}(k)$ the experimental spectrum, $\chi_{theo}(k)$ the fit spectrum, P the number of data points, and F the number of free variables. In EXAFS analysis interatomic distances (R) and CN have an uncertainty of 0.01–0.04 Å and 10–35%, respectively (Conradson, 1998; Soderholm et al., 2005). These uncertainties depend on the data quality and on the source of phase and amplitude functions used in the curve fit. The asymptotic standard deviation of CN or R (Tables 3–5) has to be added to estimate the total error of the respective variable.

Further data refinement was achieved by the Monte Carlo Target Transformation Factor Analysis (MCTFA) approach, which is described in detail by Rossberg and Scheinost (2005a,b). The three-dimensional (3-D) structure of a (sorption) complex was determined from initial guesses of the binding surface structure, the known or estimated Debye–Waller factors of its atoms, and the shift in energy threshold ΔE_0 determined from conventional EXAFS shell fitting. The structure of the sorption complex is found by modifying the position of the sorbing ion towards the binding surface, until a minimum deviation between the FEFF-calculated EXAFS spectrum at the given configuration and the experimental EXAFS spectrum is attained. The structure of the surface complex is further refined by allowing adjustment of the surface atom positions in a second step of MCTFA.

2.4. ATR-FTIR data collection and analysis

ATR-FTIR spectra were recorded using a GX 2000 spectrometer (Perkin Elmer) equipped with a diamond ATR cell (SensIR Techn. Co.) and a mercury cadmium telluride (MCT) detector. The ATR technique enabled acquisition of FTIR spectra of freshly ultra-centrifuged wet pastes without any further treatment. The spectrum of the respective supernatant was recorded for background subtraction. An aliquot of the wet ferrihydrite precipitate was spread over the optical crystal surface as a thin layer (<1 mm) and covered during the measurement to avoid evaporation of the supernatant. For each spectrum 128 scans were accumulated at a spectral resolution of 4 cm^{-1} (~1 min recording time). Reference spectra of a 0.1 M $NaHCO_3$ solution, and of U-free ferrihydrite precipitates prepared in the absence and in presence of 0.67 mM $NaHCO_3$ at pH 8.0 under N_2 atmosphere were used to validate the vibration bands of adsorbed carbonate. Second-derivative (SD) spectra were calculated using the algorithm by Savitzky-Golay implemented in the spectroscopy software.

Table 4
Fit parameters to the U L_{III}-edge EXAFS data of the simulated mine-water precipitate M2 recorded at 30 K (N_2-frozen sample) and at 295 K (unfrozen sample)

Temp. (K)	Model	Shell	CN[a]	R[b] (Å)	σ^{2}[c] (Å^2)	ΔE_0 (eV)	χ_v^{2}[d]
30	X = Al	U—O_{ax}	2*	1.798(2)	0.0017(1)	−5.7(5)	0.26
		U—O_{eq1}	2*	2.297(6)	0.0056(6)	#	
		U—O_{eq2}	3*	2.41*	0.007*	#	
		U—X	0.6(2)	2.75(1)	0.005(3)	#	
		U—Fe	0.9(2)	3.44(2)	0.01*	#	
30	X = S	U—O_{ax}	2*	1.799(2)	0.0017(1)	−5.2(5)	0.27
		U—O_{eq1}	2*	2.299(7)	0.0053(6)	#	
		U—O_{eq2}	3*	2.41*	0.007*	#	
		U—X	0.4(2)	2.68(1)	0.005(4)	#	
		U—Fe	0.9(2)	3.45(2)	0.01*	#	
30	X = Si	U—O_{ax}	2*	1.798(2)	0.0017(1)	−5.5(5)	0.26
		U—O_{eq1}	2*	2.298(6)	0.0055(6)	#	
		U—O_{eq2}	3*	2.41*	0.007*	#	
		U—X	0.6(2)	2.72(1)	0.005(3)	#	
		U—Fe	0.9(2)	3.45(2)	0.01*	#	
30	X = C	U—O_{ax}	2*	1.796(2)	0.0016(1)	−5.9(5)	0.27
		U—O_{eq1}	2*	2.296(6)	0.0056(6)	#	
		U—O_{eq2}	3*	2.41*	0.007*	#	
		U—X	1.8(8)	2.92(1)	0.005(3)	#	
		U—Fe	0.9(2)	3.45(2)	0.01*	#	
30	X = O	U—O_{ax}	2*	1.796(2)	0.0016(1)	−5.9(5)	0.26
		U—O_{eq1}	2*	2.296(5)	0.0056(6)	#	
		U—O_{eq2}	3*	2.41*	0.007*	#	
		U—X	1*	2.87(1)	0.003(1)	#	
		U—Fe	1*	3.45(2)	0.010(2)	#	
295	X = O	U—O_{ax}	2*	1.792(2)	0.0016(1)	−6.7(5)	0.25
		U—O_{eq1}	2*	2.276(5)	0.0052(5)	#	
		U—O_{eq2}	3*	2.41*	0.007*	#	
		U—X	1*	2.87(1)	0.003(1)	#	
		U—Fe	1*	3.46(2)	0.011(2)	#	

Different coordination models of backscattering atoms were tested for fitting the FT peak at $R + \Delta \sim 2.4$ Å. To reduce the number of free variables, some of them were correlated (#) or fixed (*) during the fitting. $MS_{U=O}$ path considered as described in Section 2.3. Asymptotic standard deviations are given in parentheses.

[a] Coordination number.
[b] Interatomic distance.
[c] Debye–Waller factor.
[d] Goodness-of-fit parameter according to Section 2.3., Eq. (1).

For this calculation between 25 and 49 neighboring data points were considered.

3. Results

3.1. Experimental simulation of mine flooding

Near-neutral (pH 6.5), sparsely mineralized groundwater (EC of 255 μS/cm) was added by steps of 10–20 L to acidic (pH 2.85), highly mineralized water (EC of 2090 μS/cm) from an early flooding stage of the Königstein uranium mine. The mine water was depleted in oxygen and rich in sulfate, iron (thereof 30% in the ferric form), aluminum and uranium (Table 1). Three experimental runs simulated flooding of the uranium mine at various late stages. Fig. 2 shows the result of one of the mesocosm experiments from which we collected the precipitate M2 at a final pH of 5.76. The pH increased as a function of time and mixing ratio, i.e., the volume of the mixture divided by the initial mine-water volume. The proportion of colloidal Fe increased with progressive Fe^{2+} oxidation as indicated by the declining Fe^{2+}/Fe_{tot} ratio. Colloidal Al and U appeared at pH > 4.5 in addition to the colloidal Fe, and reached relative concentrations of 95–99% at pH 6. The solid to liquid ratio (S/L) of the experimental floodwater reached 40 mg/L. This value is much lower than S/L ratios commonly used in sorption experiments.

3.2. Characterization of colloids and precipitates

3.2.1. Physical and mineralogical properties

Photon correlation spectroscopy of the mesocosm suspensions revealed a broad particle size distribution. After filtration, SEM images of a 1 μm Nucleopore® filter membrane showed particles of 70–100 nm in both isolated and aggregated forms (Fig. 3). A moderate positive zeta potential of 5–10 mV was measured below the point of zero net charge at pH 6.1 (M2) and pH 6.5 (M1) using laser Doppler electrophoresis and applying the Smoluchowski equation. The low surface charge indicates low electrostatic

Table 5
Fit parameters to the U L_{III}-edge EXAFS spectra of U-ferrihydrite coprecipitates prepared with [U_{tot}] of 12 μM at pH 5.5 (S10 + S11) and pH 8.0 (S12 + S13) at atmospheric pCO_2 of 35.5 Pa (S10 + S12) and N_2 atmosphere ($pCO_2 < 0.2$ Pa) (S11 + S13) (Fig. 6)

Sample	Shell	CN^a	R^b (Å)	σ^{2c} (Å^2)	ΔE_0 (eV)	χ_v^{2d}
S10	U=O	2*	1.793(2)	0.0024(1)	−6.2(4)	0.15
	$U-O_{eq1}$	2*	2.287(5)	0.0075(6)	#	
	$U-O_{eq2}$	3*	2.41*	0.007*	#	
	$U-O_{sf}$	1.0(3)	2.87(1)	0.004(2)	#	
	U—Fe	1*	3.395(6)	0.0062(6)	#	
	$MS_{U=O}$	2*	3.58	0.0048	#	
S11	U=O	2*	1.804(2)	0.0019(1)	−5.4(4)	0.24
	$U-O_{eq1}$	2*	2.293(5)	0.0061(6)	#	
	$U-O_{eq2}$	3*	2.41*	0.007*	#	
	$U-O_{sf}$	1*	2.87(1)	0.005(2)	#	
	U—Fe	0.8(3)	3.386(7)	0.005(2)	#	
	$MS_{U=O}$	2*	3.60	0.0038	#	
S12	U=O	2*	1.799(2)	0.0023(1)	−5.8(5)	0.23
	$U-O_{eq1}$	2*	2.289(7)	0.0083(9)	#	
	$U-O_{eq2}$	3*	2.41*	0.007*	#	
	$U-O_{sf}$	1.2(6)	2.86(1)	0.006(3)	#	
	U—Fe	1.0(5)	3.41(1)	0.009(4)	#	
	$MS_{U=O}$	2*	3.60	0.0046	#	
S13	U=O	2*	1.808(2)	0.0022(1)	−5.1(4)	0.17
	$U-O_{eq1}$	2*	2.277(5)	0.0073(6)	#	
	$U-O_{eq2}$	3*	2.41*	0.007*	#	
	$U-O_{sf}$	1.2(2)	2.89(1)	0.005*	#	
	U—Fe	1*	3.408(7)	0.0066(7)	#	
	$MS_{U=O}$	2*	3.62	0.0044	#	

To reduce the number of free variables, some of them were correlated (#) or fixed (*) during the fitting. Asymptotic standard deviations are given in parentheses.
[a] Coordination number.
[b] Interatomic distance.
[c] Debye–Waller factor.
[d] Goodness-of-fit parameter according to Section 2.3., Eq. (1).

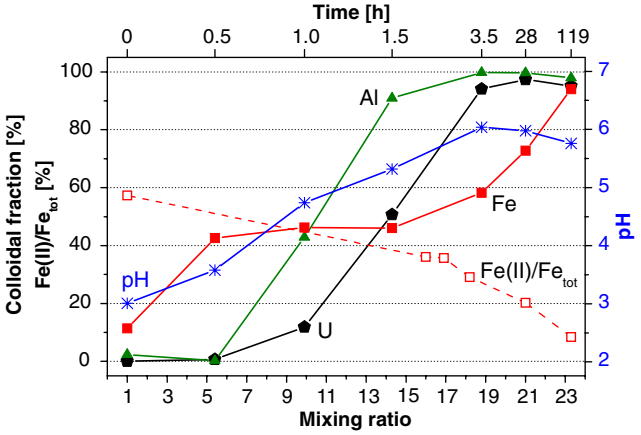

Fig. 2. Percentage of colloidal U, Al, Fe (based on 3 kD ultra-filtration), Fe(II)/Fe_{tot} fraction (left ordinate) and pH (right ordinate) as functions of mixing ratio (lower abscissa) and time (upper nonlinear abscissa) in the experimentally simulated flooding scenario.

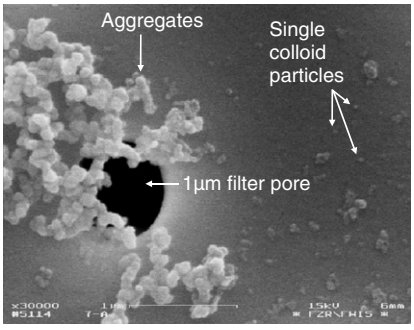

Fig. 3. SEM image (30,000×) of colloidal particles and aggregates next to a 1 μm pore in the filter membrane.

stability of the colloid particles and explains their tendency of aggregation. X-ray powder diffraction of the pulverized precipitates showed an X-ray amorphous pattern with two broad *hk* scattering bands at ~1.5 and ~2.6 Å (62° and 36° of 2*θ* scale) typical of two-line ferrihydrite (Schwertmann et al., 1999). Mössbauer spectroscopy confirmed this mineral phase and did not identify other Fe minerals on a detection limit of ~1% (unpublished data). ICP-MS bulk analysis of the HNO_3/HCl digested precipitate M2 showed the predominance of Fe (373 mg/g), besides accessory Al (56 mg/g), S (24 mg/g), U (21 mg/g), Si (14 mg/g), C (6.5 mg/g) and N (0.68 mg/g). Taking the analytical results of trace elements into account, an oxygen (O) content of ~48% was estimated. X-ray absorption spectroscopy was applied on the wet pastes at the Fe K and U L_{III} absorption

edges to obtain structural information on the nature of the freshly formed colloids and aggregates, and especially on the uranium binding at the molecular level.

3.2.2. Molecular binding by Fe K-edge EXAFS

Fig. 4 shows the Fe K-edge EXAFS and corresponding Fourier transform (FT) spectra of the ferrihydrite dominated precipitate M2 and of two ferrihydrite reference samples, S8 and S9, freshly prepared at $pCO_2 < 0.2$ Pa (Table 2). The ferrihydrite precipitate had a large surface area of 228 m^2/g (BET-N_2). The first FT peak (uncorrected for phase shifting) corresponds to five to six oxygen atoms (—O, —OH, or —OH_2 ligands) coordinated to the absorbing Fe atom by two different atomic distances (R). Up to three O-atoms were found to be coordinated with $R_{Fe—O1} \sim 1.94$ Å and $R_{Fe—O2} \sim 2.06$ Å, respectively (Table 3). The second FT peak is fit by three Fe—Fe contributions with $R_{Fe—Fe1} = 2.89$–2.96 Å, $R_{Fe—Fe2} \sim 3.07$ Å, and $R_{Fe—Fe3} = 3.37$–3.45 Å. Including a forth Fe shell with $R_{Fe—Fe4} = 3.92$–4.00 Å improved the fit of oscillations at higher k-values and explained the third FT peak, thus reducing the statistical fit error. Nevertheless, the accuracy of CN is reduced at this large radial distance due to the small contribution of the shell to the EXAFS signal and the increasing influence of noise. The adsorbed uranium in the ferrihydrite sample S8 was not detectable by Fe K-edge EXAFS, neither in the spectrum of S8 nor in the calculated difference of spectrum S8 and S9 (Fig. 4).

3.2.3. Molecular binding by U L_{III}-edge EXAFS

Applying U L_{III}-edge EXAFS on the simulated mine-water precipitate M2 in its original (unfrozen) stage at room temperature (295 K) and on a shock-frozen subsample at 30 K revealed no visible differences between both spectra (Fig. 5, upper spectra; Table 4). Thus substantial changes of the atomic environment due to the different sample preparation protocols can be ruled out. Also significant U—U interactions can be ruled out because high-Z elements would increase the backscattering amplitude at deep temperature EXAFS recording. The FT peak with the largest amplitude and the smallest R-value is caused by the two O_{ax} atoms of the UO_2^{2+} cation. Therefore the $CN_{U=O}$ was fixed to 2 and a mean radial distance $R_{U=O}$ of ~1.80 Å was calculated. The corresponding $MS_{U=O}$ path was reflected by a small FT peak at $R + \Delta \sim 2.9$ Å that was much smaller than the measured peak. This peak was perfectly fit by one Fe atom at ~3.45 Å. The tight radial distance can be explained by a bidentate (edge-sharing) linkage of the UO_2^{2+} cation to an $Fe(O,OH)_6$ octahedron, which is consistent with the formation of an inner-sphere complex on the ferrihydrite surface (e.g., Waite et al., 1994; Dodge et al., 2002). The second FT peak was explained by the equatorial U—O_{eq} shell with CN of five, radial distance of 2.36 Å and σ^2 of 0.012 $Å^2$. This unusually high Debye–Waller factor suggests static disorder of the U—O_{eq} shell and high variation of the radial distances. Considering the above mentioned bidentate coordination of uranyl to the ferrihydrite surface, three O_{eq} atoms are assumed to be coordinated with water molecules from the initial hydration sphere. Therefore, three O_{eq} atoms were fixed with $R_{U—O_{eq}}$ of 2.41 Å and σ^2 of 0.007 $Å^2$, representing average values of pentahydrated $UO_{2(aq)}^{2+}$ (Allen et al., 1997; Sémon et al., 2001). The other two O_{eq} atoms fit to radial distances of ~2.30 Å and σ^2 of ~0.0055 $Å^2$ (Table 4), suggesting a splitting of the equatorial oxygen shell into two subshells.

Two small FT peaks at $R + \Delta \sim 2.4$ Å and ~3.8 Å (see guidelines in Fig. 5B) remain to be explained. Given the elemental composition of the simulated mine-water precipitate M2, the atoms Al, S, Si, C, N and O were considered

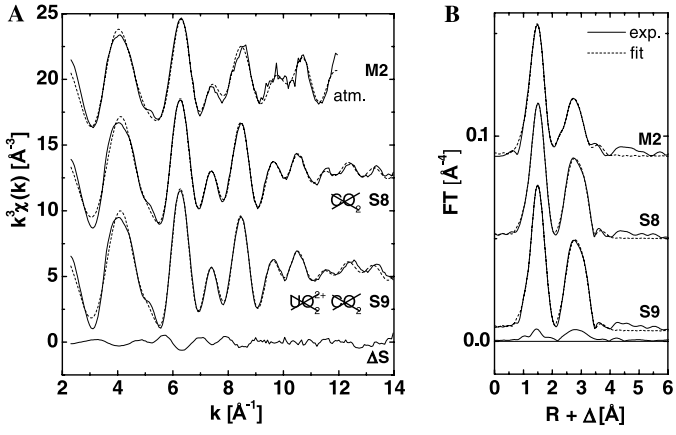

Fig. 4. (A) Fe K-edge EXAFS spectra and (B) corresponding FT's of the simulated mine-water precipitate (M2) and of two ferrihydrite reference samples (S9: without UO_2^{2+}, S8: coprecipitated with 50 μM UO_2^{2+}) prepared at CO_2-free atmosphere ($pCO_2 < 0.2$ Pa). Solid lines: experimental data, dashed lines: shell-fitting data. The difference spectrum (ΔS = S8–S9) and its corresponding FT demonstrates the absence of a significant contribution of adsorbed U(VI) to the Fe K-edge EXAFS spectrum of ferrihydrite.

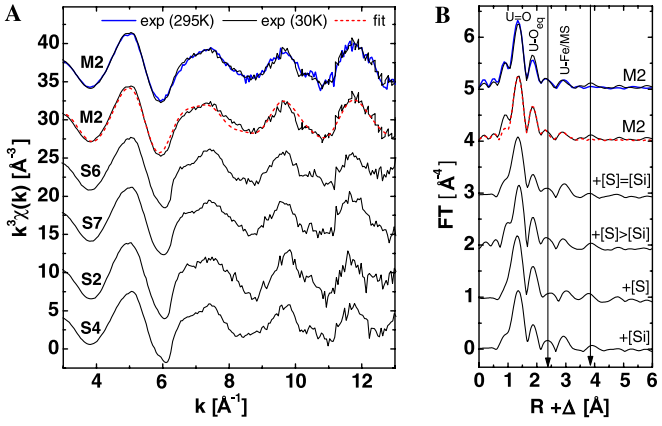

Fig. 5. (A) U L_{III}-edge EXAFS spectra and (B) corresponding FT's of the simulated mine-water precipitate M2 and of four selected samples of the sorption experiments S1–S7 (Table 1), collected at 30 K. For comparison, the room-temperature spectrum of M2 (blue solid line) is plotted on the top of the corresponding 30-K spectrum. The fit to M2 (red dotted line) is based on a Si shell in the third coordination sphere (see Table 4).

potential candidates and thus tested to fit the FT peak at $R + \Delta \sim 2.4$ Å (Table 4). Fitting this peak by an Al or S shell yielded radial distances of 2.75 Å for U—Al and 2.68 Å for U—S which is not likely, since it would indicate Al or S atoms in the first coordination sphere of U. Fitting the FT peak with a Si or C shell yielded radial distances of $R_{U-Si} = 2.72$ Å and $R_{U-C} = 2.92$ Å that are in accordance with bidentate linkage of silicate or carbonate ions to the equatorial plane of UO_2^{2+} (see Fig. 1 and Section 4). The very low content of nitrogen (N) and the N/U mole ratio of ~0.5 make the detection of an inner-sphere U—N interaction unlikely. The FT peak that can be fit by an O-shell at 2.87 Å (Table 4) though a structural model to explain this U—O distance is missing. The unique identity of the backscatterer cannot be ascertained on the basis of fit quality because the χ^2_v values do not differ significantly. Other approaches are needed to narrow down the atomic identity since the scattering amplitudes from neighboring atoms on the periodic table give similar EXAFS contribution.

One possible approach is to simplify the chemical system. Sorption/coprecipitation experiments were conducted with U(VI)-ferrihydrite in the absence and presence of sulfate, silicate, and carbonate (Table 2). The precipitates S1–S13 were also investigated by U L_{III}-edge EXAFS spectroscopy. The coprecipitation of U(VI) and ferrihydrite was performed at different concentrations of sulfate and silicate. The U L_{III}-edge EXAFS and corresponding FT spectra of these batch samples closely resemble those of the mine-water precipitate M2 (Fig. 5). The FT peaks at $R + \Delta \sim 2.4$ and ~3.8 Å occurred in all spectra, irrespective of the presence or the absence of sulfate or silicate. Furthermore, even in the absence of both components, spectral differences were not detectable (Fig. 6, S10). This suggests that the spectral signature of these samples was most likely due to another component. Since we can exclude the background electrolyte nitrate (see Section 2.2), carbonate was the key candidate to be tested more thoroughly.

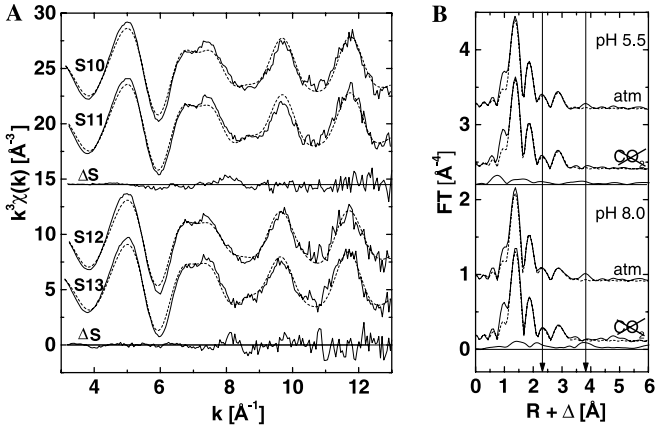

Fig. 6. (A) U L_{III}-edge EXAFS spectra and (B) corresponding FT's of selected sorption experiments. S10: pH 5.5, atmospheric pCO_2 of 35.5 Pa; S11: pH 5.5, $pCO_2 < 0.2$ Pa; S12: pH 8.0, atmospheric pCO_2 of 35.5 Pa; S13: pH 8.0, $pCO_2 < 0.2$ Pa. Solid lines: experimental data, dashed lines: shell-fitting data. ΔS: calculated difference spectra (S10–S11, S12–S13) and their corresponding FT's demonstrate the influence of pCO_2.

The influence of carbonate (in equilibrium with atmospheric pCO_2 of 35.5 Pa) on the binding of U(VI) to colloidal ferrihydrite was investigated at pH 5.5 and 8.0. Samples S10 and S11 prepared in the presence and in the absence of atmospheric CO_2 at pH 5.5, showed rather similar EXAFS spectra, and the corresponding samples at pH 8.0 differed slightly in the k-range 7.5–9.0 Å^{-1} (Fig. 6). The oscillation curve of S13 is more steep than the one of S12 at about 7.5–8.4 Å^{-1}, and is followed by a small peak at ~8.5–9.0 Å^{-1} which is absent in S12. This effect is probably weaker in S11. Whereas the FT shows a weak difference for $\Delta S = (S10–S11)$, clear backscattering contribution to the FT peaks in question is visible for $\Delta S = (S12–S13)$ (Fig. 6). The FT peak at $R + \Delta \sim 2.2$ Å in the difference spectrum may reflect a carbon shell. The FT peak at $R + \Delta \sim 3.8$ Å may arise from single scattering of the distal carbonate O-atom (U—O_{dis}), from multiple scattering of the three-legged U—C—O_{dis} path and from the four-legged U—C—O_{dis}—C path, if one assumes a bidentate coordination of carbonate to the equatorial U(VI) oxygen atoms (Bernhard et al., 2001). The signal may serve as a fingerprint for ternary uranyl-carbonato complexation on ferrihydrite at higher pH values, which are coupled with higher (bi-)carbonate equilibrium concentrations. However, the signal is weak and the fit parameters and degrees of freedom are too numerous to apply shell fitting.

In contrast to the FT peak at $R + \Delta \sim 3.8$ Å, the peak at $R + \Delta \sim 2.4$ Å appeared also in the sample spectra of the CO_2-free system (Fig. 6, S11 and S13). Under these chemical conditions, a carbon shell cannot explain the FT peak at $R + \Delta \sim 2.4$ Å. Therefore we applied MCTFA to test whether the experimental EXAFS spectrum of sample S11 could be explained by U(VI) adsorption without a contribution of other ligands (Rossberg and Scheinost, 2005a,b). During the first run of MCTFA a cluster of four $Fe(O,OH)_6$ octahedra was used, composed of face-sharing, edge-sharing, and corner-sharing coordination analogous to the structure of hematite (Blake et al., 1966). This cluster simulated different binding sites on the ferrihydrite surface. MCTFA was carried out by two steps: (i) the determination of the surface complex structure, i.e., the orientation of U(VI) towards the surface of this cluster, and (ii) the refinement of the surface complex structure by allowing the atoms of the cluster to float in relation to U(VI).

The first simulation step was based on the structural constraints of UO_2^{2+} having two fixed O_{ax} atoms ($R_{U=O} = 1.80$ Å and $\sigma^2 = 0.0018$ Å^2), and being surrounded by three water molecules at a fixed U—O_{eq} distance of 2.41 Å. The Debye–Waller factor of all O-atoms except O_{ax} was set to 0.012 Å^2, and Fe atoms was set to 0.008 Å^2 to allow sufficient flexibility of the initial structural model. The $MS_{U=O}$ path was also considered by the simulation procedure. These constraints and the parameterized EXAFS equation were used to calculate theoretical EXAFS spectra for random positions of UO_2^{2+} relative

to the $Fe(O,OH)_6$ cluster. The UO_2^{2+} ion was moved in a sphere of 14 Å in diameter, with the origin of the sphere set to the estimated geometric center of the chosen cluster. Theoretical EXAFS spectra of about 4.7×10^6 tested random positions of UO_2^{2+} were calculated and compared with the experimental EXAFS spectrum by standard deviation. The solution set of standard deviations showed two minima representing two statistically most likely positions of UO_2^{2+} on the $Fe(O,OH)_6$ cluster (Fig. 7B). Both positions are very similar, representing a bidentate (edge-sharing) coordination of U(VI) to one Fe octahedron. Since ~95% of the experimental spectrum (Fig. 7A) is explained by backscattering contributions from one $Fe(O,OH)_6$ octahedron, one of both configurations was selected for the second step to reduce computing time.

During the second step of MCTFA, the structural disorder of the backscattering atoms was statistically simulated by creating a large number of (initially) identical U(VI) sorption complexes (Rossberg and Scheinost, 2005b). The position of the U-atom was fixed for each of the complexes, while all neighboring Fe and O-atoms were randomly moved, including the O_{ax} atoms and the corresponding $MS_{U=O}$ paths. This calculation produced a refined complex structure, with the standard deviation decreasing from 0.41 (step 1) to 0.32 (step 2). Fig. 7C demonstrates the excellent fit of the experimental spectrum by the MCTFA-refined structure. Fig. 7D shows the resulting 3-D structure where the UO_2^{2+} ion is bidentately bound to one $Fe(O,OH)_6$ octahedron with radial distances of $R_{U-O_{eq1}} \sim 2.30$ Å, R_{U-Fe} ~3.40 Å, and a distance of 2.84 Å to the apical O-atom of the $Fe(O,OH)_6$ octahedron. An unexpected feature of this topology is that the equatorial plane of the $[UO_2(H_2O)_5]^{2+}$ pentagonal bipyramid and the equatorial square plane of the edge-sharing $Fe(O,OH)_6$ octahedron are slightly tilted at an angle of ~32°, so that one of the O_{ax} atoms would approach close to the surface hydroxyl group.

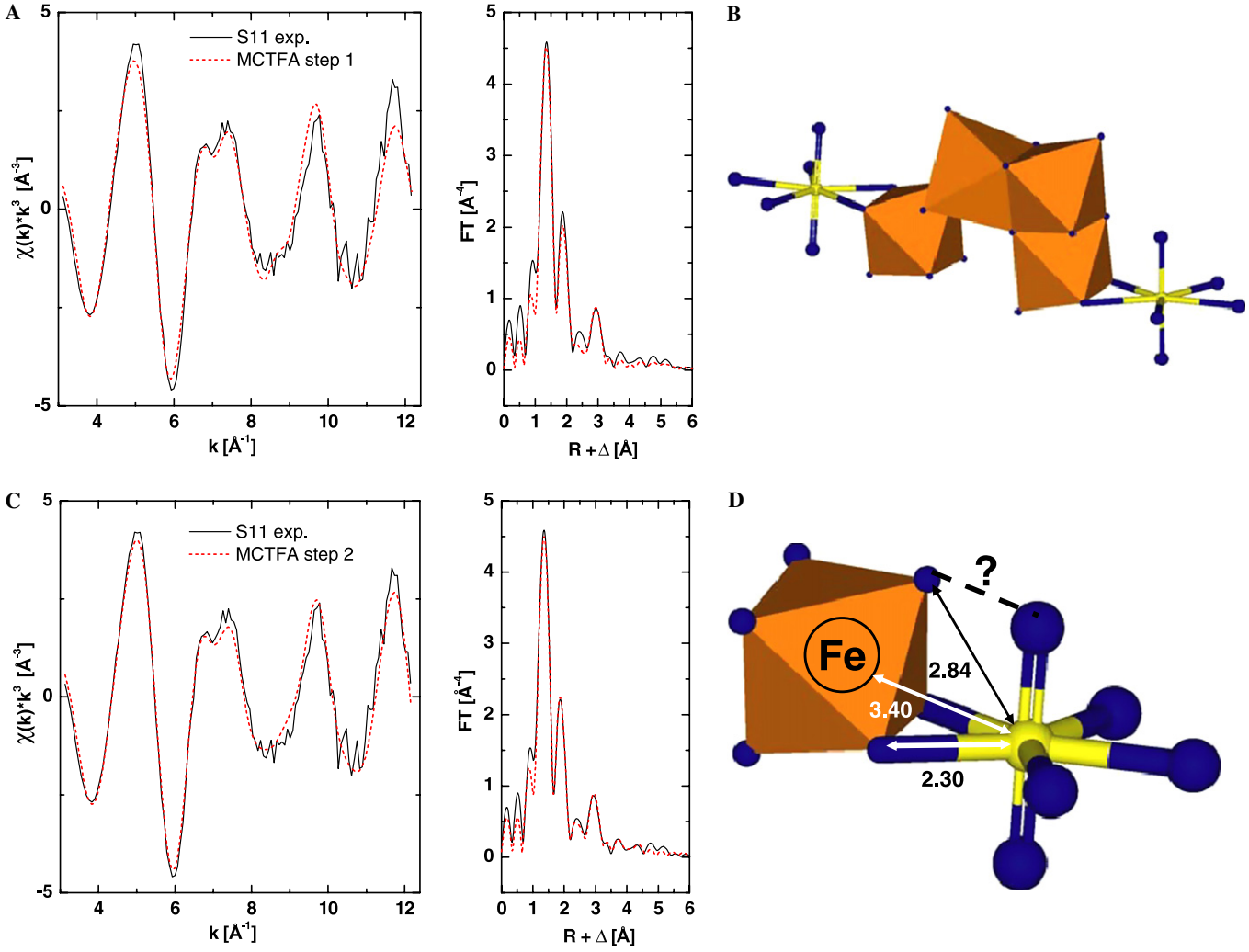

Fig. 7. Result of the Monte Carlo Transformation Factor Analysis (MCTFA) of sample S11 (pH 5.5, $pCO_2 < 0.2$ Pa). Experimental U L_{III}-edge EXAFS spectrum (solid line) and MCTFA fit (dashed line). (A) After first MCTFA step, (C) after second MCTFA step, (B) and (D) corresponding structures. Numbers in (D) give interatomic distances in Ångström. The MCTFA fit in panel C corresponds to the coordination of U(VI) at the left side of the sketch in panel B. For further explanations see text.

3.2.4. Molecular binding by ATR-FTIR

The spectrum of a U-free ferrihydrite precipitate prepared at pH 5.5 and $pCO_2 < 0.2$ Pa, i.e., without adsorption of U(VI) and carbonate, shows a broad absorption band in the regions of 937 cm^{-1} representing the δ(OH) bending vibration of the ferrihydrite phase (Fig. 8A, middle). The spectra of ferrihydrite samples containing UO_2^{2+} ions exhibit an additional band at ~903 cm^{-1}, the intensity of which correlates with increasing U(VI) concentration (Fig. 8C–E, middle). This band represents the antisymmetric stretching vibration (v_3) of the UO_2^{2+} cation adsorbed to the Fe hydroxide phase. Contrary to the samples prepared at atmospheric pCO_2 of 35.5 Pa, the spectra of both samples prepared while excluding CO_2 from the system have no absorption bands in the range of 1250–1600 cm^{-1}, thus verifying the absence of adsorbed carbonate (Fig. 8A and F, left). The other sample spectra show additional bands around 1365 and 1500 cm^{-1} (Fig. 8B–E, left) which are due to the symmetric (v_s) and antisymmetric (v_{as}) stretching vibration of carbonate ligands bound to the ferrihydrite phase. These bands show a steady shift to higher wavenumbers with increasing U(VI) concentration. In particular the frequency of the $v_{as}(CO_3^{2-})$ vibration shifts from 1478 to 1515 cm^{-1}, the latter being reached by the sample prepared with initially 0.1 mM UO_2^{2+}. A similar, but smaller shift from 1365 to 1372 cm^{-1} was observed for the $v_s(CO_3^{2-})$ vibration ($\Delta v_s \sim 7$ cm^{-1}; Fig. 8E, left).

The second derivative (SD) spectra were calculated in the spectral region of 1600–1250 cm^{-1} (Fig. 8, right) to elucidate the peak positions of overlapping carbonate bands. The SD maxima indicate the peak positions of components underlying the bands in the ATR spectra. In homology to the ATR spectrum of U-free ferrihydrite the band position in the SD spectrum of the $v_{as}(CO_3^{2-})$ is again found at 1478 cm^{-1} (Fig. 8B, right) indicating no overlapping bands in this spectral region. However, the band position of the $v_{as}(CO_3^{2-})$ shifted to 1488 cm^{-1} when ferrihydrite was prepared in the presence of 0.012 mM UO_2^{2+} (Fig. 8C, right). The intensity of this band decreased with increasing UO_2^{2+} concentration, whereas a band at 1521 cm^{-1} became larger with higher UO_2^{2+} concentrations (Fig. 8C–E, right). This band corresponds to the maximum of the $v_{as}(CO_3^{2-})$ band at 1515 cm^{-1} found in the respective ATR spectrum

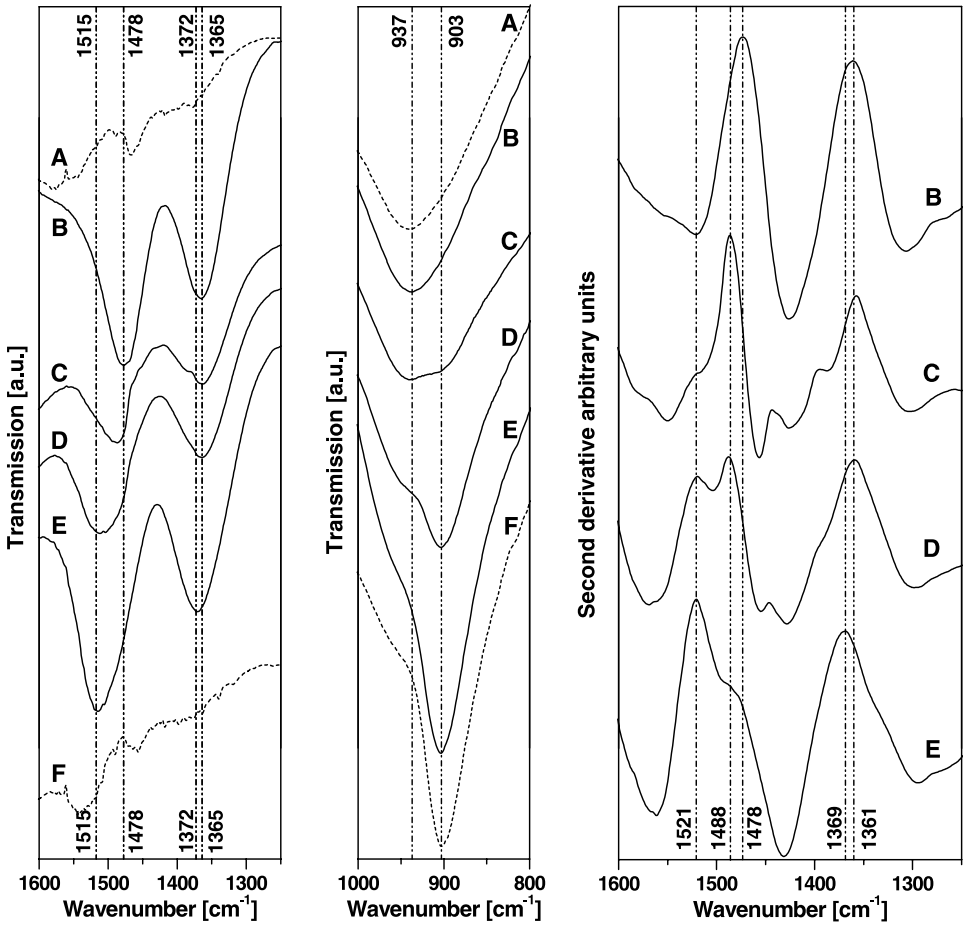

Fig. 8. ATR-FTIR spectra of U(VI) sorption samples prepared at pH 5.5 and different UO_2^{2+} concentrations. A, F: samples prepared at $pCO_2 < 0.2$ Pa; (B–E) samples prepared at atmospheric pCO_2 of 35.5 Pa. Shown are the region of the carbonate stretching vibrations (left), the region of the uranyl stretching vibration (middle), and the second derivative spectra of the carbonate stretching region (right). Initial UO_2^{2+} concentrations were: 0 mM (A and B); 0.012 mM (C); 0.05 mM (D); 0.1 mM (E and F).

(Fig. 8E, left). In conformity with the ATR spectra the $\nu_s(CO_3^{2-})$ band of the SD spectra shows small deviations with increasing UO_2^{2+} concentration (1361–1369 cm^{-1}). Nevertheless, in the spectrum of the ferrihydrite precipitate containing 0.1 mM UO_2^{2+} the position is shifted slightly towards higher wavenumbers (Fig. 8E, right).

4. Discussion

4.1. Molecular structure of the ferrihydrite precipitates

Initial polymers in a ferric nitrate solution are characterized by six (O, OH, OH_2)-ligands in the first coordination shell of Fe at an average distance of 1.97 Å (Combes et al., 1989). After adding hydroxyl ions at a mole ratio OH/Fe $\geqslant$ 2.5, the first oxygen shell splits into two subshells separated by ~0.12 Å (Table 3) which is close to the limit of distance resolution. However, a similar splitting in two Fe—O distances of 1.95 Å and 2.06 Å was observed by Rose et al. (1997) and may be interpreted as a result of the presence of Fe—O and Fe—OH bonds, respectively (Combes et al., 1989), indicating the formation of slightly distorted octahedral clusters by deprotonation. The fit Fe—Fe contributions then allow to determine the type of molecular linkage between these Fe octahedra. Face-sharing octahedra have typical Fe—Fe distances of 2.85–2.94 Å, and edge-sharing octahedra have Fe—Fe distances of 2.95–3.10 Å (Combes et al., 1990). An interatomic Fe—Fe distance of 3.37–3.45 Å indicates double-corner sharing of Fe octahedra (Combes et al., 1989; Rose et al., 1997). A Fe—Fe distance of 3.92–4.00 Å indicates a bond between two Fe octahedra sharing one corner (Manceau and Drits, 1993).

The Fe—Fe_1 distance of 2.89 Å (Table 3) found in the simulated mine-water precipitate M2 is characteristic of face-sharing octahedra known from the local structures of hematite (Blake et al., 1966), feroxyhyte (Drits et al., 1993a), and defective ferrihydrite, that is an intermediate phase between periodic ferrihydrite and hematite (Drits et al., 1993b; Janney et al., 2000). The structural data of M2, in particular the *CN* values of the face-sharing ($CN = 1$) and edge-sharing ($CN \sim 3$) Fe—Fe contributions as well as the Fe—Fe_3 distance of 3.37 Å (double-corner linkage) match the EXAFS data derived from highly polymerized intermediate stages during the transformation of freshly precipitated Fe gels to hematite (Combes et al., 1990). Considering the number of face, edge and double-corner sharing octahedra of common Fe oxyhydroxides on the local scale of EXAFS, hematite is characterized by 1, 3, and 3, which is more similar to the structure of M2 with 1, ~3, and ~1 (Table 3) than α/β-FeOOH (0, 4, 4) or γ-FeOOH (0, 6, 0; plus two single-corner sharing octahedra) (Manceau and Drits, 1993). Therefore, we used the unit cell cluster of hematite (Blake et al., 1966) when applying the MCTFA approach (Fig. 7B).

In contrast to the ferrihydrite dominated precipitate M2, the ferrihydrite reference samples reveal a Fe—Fe_1 distance of 2.94–2.96 Å (Table 3), which cannot be unequivocally attributed to either face-sharing or edge-sharing linkage. A Fe—Fe_1 distance of 2.95 Å has been determined from EXAFS spectra of hematite, where the spectra are modeled as an average of face-sharing ($R_{Fe—Fe} = 2.90$ Å, $CN = 1$) and edge-sharing ($R_{Fe—Fe} = 2.97$ Å, $CN = 3$) shells, due to the low spatial resolution (Manceau and Combes, 1988). In this case, the combined *CN* would be 4 in hematite, which is much higher than the *CN* value derived from our spectra ($CN \sim 0.5$; Table 3). An additional Fe—Fe shell with $R_{Fe—Fe2}$ ~3.07 Å was found, indicating edge-sharing linkage. Therefore, the average local structure of our ferrihydrite samples is different from the crystal structure of hematite. Rose et al. (1997) investigated the structural evolution of oligomers in partially hydrolyzed ferric nitrate solutions by EXAFS spectroscopy and found Fe—Fe shells with similar distances, but with slightly different *CN* values. Our structural EXAFS data (Table 3) support a local molecular structure consisting of at least six Fe(O,OH) octahedra (Fe_6 cluster) forming the basic unit (Fig. 9). In analogy to the tetrameric unit proposed for 2-line ferrihydrite (Feitknecht et al., 1973), one of the most likely configurations for such a Fe_6 cluster is a planar linkage by edges of four Fe octahedra, to which two other Fe octahedra are attached by sharing double-corners. This basic unit forms a homogeneous network by sharing single corners with two other modules of the same type. The average *CN* values of the Fe atoms in the Fe_6 cluster (Table 6) are close to the values determined from the experimental EXAFS data (Table 3), taking into account the presence of neighboring clusters. According to this topological approach, the experimental EXAFS data of precipitated

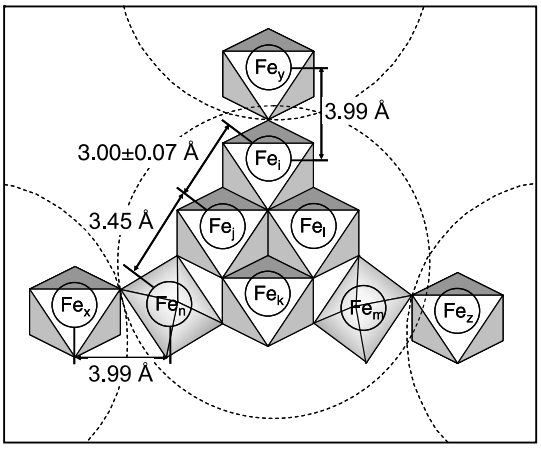

Fig. 9. Sketch of the local structure of ferrihydrite based on the experimental EXAFS data of the precipitation samples (Fig. 4, spectra S8 and S9; Table 6). The basic unit (indicated by dashed circles) consists of six $Fe(O,OH)_6$ octahedra in planar arrangement; four of them are coordinated by edges (with Fe—Fe distances of 3.00 ± 0.07 Å), and two octahedra are linked to this tetrameric unit by sharing double-corners (with Fe—Fe distances of 3.45 Å). Each basic unit representing a section of the homogenous network is linked to two other modules of the same type by sharing a single corner with Fe—Fe distances of 3.99 Å (modified from Rose et al., 1997).

Table 6
Coordination numbers (*CN*) for the Fe_6 cluster ($n_{Fe} = 6$) depicted in Fig. 9

	$CN_{Fe1/Fe2}$ (3.00 ± 0.07 Å)	CN_{Fe3} (3.45 Å)	CN_{Fe4} (3.99 Å)
Fe_i	2 (Fe_j–Fe_l)	0	1 (Fe_y)
Fe_j	3 (Fe_i–Fe_k–Fe_l)	1 (Fe_n)	0
Fe_k	2 (Fe_j–Fe_l)	2 (Fe_m–Fe_n)	0
Fe_l	3 (Fe_i–Fe_j–Fe_k)	1 (Fe_m)	0
Fe_m	0	2 (Fe_k–Fe_l)	1 (Fe_z)
Fe_n	0	2 (Fe_j–Fe_k)	0
$CN_{calc} = \sum CN/n_{Fe}$	1.67	1.33	0.33
CN_{fit} (Sample S8 + S9)	1.65 ± 0.15	1.3 ± 0.2	0.3

2-line ferrihydrite are consistent with a network of Fe_6 clusters. A statistically representative section is shown in Fig. 9.

4.2. U(VI) coordination to ferrihydrite

For both the freshly formed mine-water precipitate M2 and the U(VI)-loaded ferrihydrite reference samples, the fitting of the first and second oxygen shell of the U L_{III}-edge EXAFS spectra (Figs. 5 and 6) yielded two oxygen atoms at a distance of ~1.80 Å (U═O) and about five oxygen atoms at 2.30–2.41 Å (U—O_{eq1}, U—O_{eq2}). The fits are in good agreement with the local structure of uranyl hydrate, verifying the hexavalent state of uranium (Burns et al., 1997).

The forth FT peak at $R + \Delta \sim 2.9$ Å was explained by two contributions, the $MS_{U=O}$ path comprising up to 10% of the peak, and the single scattering of one Fe atom at $R_{U-Fe} = 3.39$–3.46 Å. This result is consistent with a mononuclear inner-sphere edge-sharing linkage of UO_2^{2+} and (hydrous) ferric oxides. The same type of coordination has been previously found for ferrihydrite (Waite et al., 1994; Reich et al., 1998; Dodge et al., 2002), lepidocrocite (γ-FeOOH) (Moyes et al., 2000; Dodge et al., 2002), goethite (α-FeOOH) (Moyes et al., 2000; Walter et al., 2003), and hematite (Bargar et al., 2000; Duff et al., 2002). Duff et al. (2002) point out that a U—Fe distance of ~3.45 Å may result from the adsorption of U(VI) to edges of face-sharing octahedra that have a longer Fe—O bond distance of 2.12 Å due to a substantial distortion, as compared to unshared faces with Fe—O bond distances of 1.95 Å. A similar distortion, but with Fe—O bond distances not exceeding 2.06 Å, is found in our ferrihydrite samples (Table 3). As for the equatorial oxygen shell of U(VI) sorbed (hydrous) ferric oxides, previous EXAFS investigations mostly found two different bond lengths, a short $R_{U-O_{eq1}}$ of 2.2–2.3 Å, and a longer $R_{U-O_{eq2}}$ of 2.4–2.5 Å. While Waite et al. (1994) and Dodge et al. (2002) suggested the edge-sharing coordination of U(VI) to the $Fe(O,OH)_6$ octahedron to be represented by the longer U—O_{eq} distance of 2.52 Å and 2.54 Å, Duff et al. (2002) and Bargar et al. (2000) used the shorter U—O_{eq} distances of 2.21 Å and 2.32 Å in their molecular models (cf. Fig. 1C). Both the MCTFA fit and the shell fit of the EXAFS data are consistent with a molecular model in which the shorter U—O_{eq} bonds point towards the ferrihydrite surface, and the longer bonds point away from the surface, attributed to coordinated H_2O molecules.

Besides the U—Fe shell explaining the forth FT peak at $R + \Delta \sim 2.9$ Å, additional contribution of a U—Al shell cannot be excluded for the simulated mine-water precipitate M2 that contained accessory Al (56 mg g^{-1} dry matter). Investigating U(VI) adsorption onto montmorillonite, Hennig et al. (2002) explained their fit results ($R_{U-Al} = 3.40$–3.44 Å, $CN = 0.5$–0.8) by a mononuclear inner-sphere complex with bidentate coordination of uranyl to hydroxylated aluminol (Al-OH) edge sites. While montmorillonite was not detected by X-ray powder diffraction in M2, X-ray amorphous Al-hydroxide phases are attended to form at the experimental pH of mine flooding (pH 5–6, Fig. 2). Thus sorption of U(VI) to these phases cannot be ruled out.

Occlusion of U(VI) in the ferrihydrite structure might have been an alternative retention mechanisms for U(VI), besides the formation of inner-sphere sorption complexes (Duff et al., 2002). While the structure of the uranyl unit with two double-bond O atoms is not compatible with the local structure of Fe oxyhydroxides, uranate U(VI) with spherical symmetry and a much smaller ion radius of 0.7 to 0.8 Å can be incorporated in small amounts (mole ratio U/Fe <0.004). The mole ratio of M2 is 0.013, thus approximately one third of U(VI) could be hosted in the ferrihydrite structure. In this case, however, four to six U—Fe neighbors and a significant *CN* reduction of the U═O shell would have been found (Duff et al., 2002). Only one U—Fe neighbor (Tables 4 and 5) provides strong evidence for adsorbed rather than incorporated U(VI) species. Likewise, neither EXAFS nor X-ray powder diffraction revealed evidence of surface precipitation of U(VI) up to $[U_{tot}]$ of 0.05 M. The EXAFS spectra did not show backscattering U—U interactions within the near atomic environment, and diffraction patterns of uranium minerals such as metaschoepite, liebigite or uranophane were not observed.

4.3. Ternary U(VI) sorption species on ferrihydrite: sulfate and silicate ligands

Since ionic sulfate and silicate species are ubiquitous in acidic mine waters, formation of ternary U(VI) sorption complexes involving these ions has to be considered. Typical U—S radial distances reported in the literature are 3.07 Å as in the solid $UO_2SO_4 \cdot CH_3CON(CH_3)_2$ (Blatov et al., 1990), and 3.11–3.14 Å as in a mixture of aqueous $UO_2SO_4^0$ and $UO_2(SO_4)_2^{2-}$ (Moll et al., 2000). A distance of 3.67 Å was found for U(VI) sorbed schwertmannite and was explained by two inner-sphere complexes with either mononuclear monodentate or binuclear bidentate linkage (Walter et al., 2003). In samples M2, S2, S6 and S7, the sulfur shell fit yielded $R_{U-S} \sim 2.68$ Å (Table 4), which is much smaller than distances reported for bidentate coordination of sulfate to the equatorial U(VI) oxygens, and would

expand the O—S—O tetrahedral angle from 109.5° to 118° (Fig. 1A), which is unlikely.

Contrary to the sulfate ligands, the calculated EXAFS data are consistent with a bidentate (edge-sharing) linkage of silicate to the equatorial U(VI) oxygen atoms at $R_{U-Si} \sim 2.72$ Å (Fig. 1B), a coordination model that has been proposed by Reich et al. (1998) and Moyes et al. (2000) for U(VI) sorbed silica gel and muscovite. Neglecting the ongoing discussion on this model, the CN_{U-Si} should be a function of Si uptake. However, no change of CN_{U-Si} was found with increasing Si uptake (0, 0.05, 0.19, 0.39 mM, Table 2) in the U(VI) sorption experiments with ferrihydrite. Note that the EXAFS spectra of U(VI) sorption samples prepared in absence of silica could be fit with a U—Si shell at $R_{U-Si} \sim 2.72$ Å. Hence fitting this FT peak with Si is not consistent, and other chemical components of the system had to be checked. Furthermore, there was no evidence of coprecipitation or trapping of U(VI)—Si complexes while ferrihydrite precipitation similar to that described by Allard et al. (1999).

4.4. Ternary U(VI) sorption species on ferrihydrite: carbonate ligands

Fitting the FT peak at $R + \Delta \sim 2.4$ Å by a U—C shell at 2.92 Å is in line with a bidentate linkage of carbonate to the equatorial U(VI) oxygen atoms (Fig. 1C). EXAFS data of $R_{U-C} = 2.88$ Å and $CN = 3$ match the structures of $UO_2(CO_3)_{3(aq)}^{4-}$ (Bargar et al., 2000) and $Ca_2UO_2(CO_3)_{3(aq)}$ (Bernhard et al., 2001). Similar interatomic U—C distances in the range of 2.81–2.92 Å were reported for the U(VI) carbonate minerals liebigite $Ca_2(UO_2)(CO_3)_3 \cdot 11H_2O$, cejkaite $Na_4(UO_2)(CO_3)_3$, zellerite $CaUO_2(CO_3)_2 \cdot 5H_2O$, and rutherfordine UO_2CO_3 (Catalano and Brown, 2004). Reich et al. (1998) found in a study on U(VI) sorption to ferrihydrite that the fits of the recorded EXAFS spectra improved when adding one carbon shell with $R_{U-C} = 2.93$ Å. Using similar experimental conditions as in this study, i.e., initial U concentrations of 10–12 μM, pH 4.5–8.2, ambient atmosphere, but hematite instead of ferrihydrite as the sorbate, Bargar et al. (1999, 2000) suggested ternary sorption complexes with bidentate coordination of carbonate to the equatorial U(VI) oxygen atoms for the whole pH range tested. This conclusion was based on EXAFS spectra showing a FT peak at $R + \Delta \sim 2.3$ Å, and supported by electrophoretic mobility measurements, and ATR-FTIR spectroscopy. However, at atmospheric pCO_2 of 35.5 Pa, the equilibrium concentrations of HCO_3^- (<2 μM) and $CO_{2(aq)}$ (10.7 μM) are low at pH 5.5, suggesting the proposed ternary complex structure is not very likely at pH below 5.5.

One carbonate ligand in bidentate coordination to U(VI) (Fig. 1C) should generate a significant peak in the EXAFS FT spectrum at $R \sim 4.3$ Å due to the single scattering of the O_{dis} atom of carbonate and the multiple scattering of U—C—O_{dis} and U—C—O_{dis}—C paths. In fact, a peak at $R + \Delta \sim 3.8$ Å was observed when samples were prepared at ambient atmosphere, i.e., without exclusion of CO_2 (Figs. 5 and 6). Furthermore, the signal was larger at pH 8.0 than at pH 5.5, in line with the expected formation of aqueous uranylcarbonato species. This supports the formation of ternary carbonate sorption complexes at the investigated conditions ([U_{tot}] of 12 μM, pCO_2 of 35.5 Pa), with a bidentate coordination of carbonate to the adsorbed U(VI). Note that it may not be possible to discriminate a monodentate linkage of carbonate, because the backscattering signal expected at $R_{U-C} \sim 3.58$ Å (rutherfordine) would be very low and most likely hidden by the stronger U—Fe shell. Therefore, ATR-FTIR spectroscopy was used as a complementary method.

In equilibrium with atmospheric pCO_2 of 35.5 Pa and in the absence of adsorbed UO_2^{2+}, carbonate ions strongly adsorb to ferrihydrite. This can be derived from the ~1478/1361 cm^{-1} and ~1482/1355 cm^{-1} $\nu_{as/s}(CO_3^{2-})$ vibrational bands in the pH 5.5 (Fig. 8B, right) and pH 8 sample spectra (not shown here). The band positions and in particular the degree of splitting between the symmetric and antisymmetric stretching modes have previously been assigned to inner-sphere mononuclear monodentate carbonate complexes (Su and Suarez, 1997; Villalobos and Leckie, 2001), and were confirmed by *ab initio* calculations (see Lefèvre, 2004). Bargar et al. (2005) recently investigated carbonate surface complexes on hematite by ATR-FTIR spectroscopy and compared vibrational frequencies of deconvoluted spectra with values calculated for conceptual binding models. The authors suggest two major complex species coexisting at near-neutral pH, one of which is attributed to the experimentally observed ~1477/1354 cm^{-1} $\nu_{as/s}(CO_3^{2-})$ bands being in accordance with our result. Bargar et al. (2005) propose an outer-sphere or hydrogen bonded carbonate complex closely associated with the hematite surface.

The $\nu_{as/s}(CO_3^{2-})$ modes shifted to a higher wavenumber of ~1521 cm^{-1} when UO_2^{2+} cations were present in the system and adsorbed to the initially colloidal ferrihydrite in competition with carbonate ions originating from atmospheric CO_2 (Fig. 8C–E, right). This observation was made at pH 5.5 and 8.0. Given the degree of splitting ($\Delta\nu_{as/s}$) as a criterion to differentiate between monodentate mononuclear (single-corner sharing), bidentate mononuclear (edge-sharing), and monodentate binuclear (double-corner sharing) complexes (Lefèvre, 2004), the increase of $\Delta\nu_{as/s}$ in the presence of adsorbed uranyl (152–176 cm^{-1} at pH 5.5 and pH 8.0) ranges between the $\Delta\nu_{as/s}$ value of the $UO_2(CO_3)_3^{4-}$ complex ($\Delta\nu_{as/s} = 140$ cm^{-1}) and the mineral andersonite ($Na_2Ca[UO_2(CO_3)_3] \cdot 6H_2O$, $\Delta\nu_{as/s} \sim 190$ cm^{-1}; Amayri et al., 2004). In both complexes the carbonate group is bidentately coordinated to UO_2^{2+} in the equatorial plane. According to Bargar et al. (1999), monodentate coordination of carbonate ligands to U(VI) should give rise to $\Delta\nu_{as/s}$ values smaller than those for bidentate coordination, i.e., <140 cm^{-1}. For instance, the decrease of $\Delta\nu_{as/s}$ from ~164 cm^{-1} to ~110 cm^{-1} by competitive adsorption of carbonate and lead (Pb^{2+}) to goethite (α-FeOOH) was

attributed to the formation of a metal-bridged ternary complex with monodentate linkage of carbonate and Pb^{2+} adsorbed onto the goethite surface (Ostergren et al., 2000).

Hence the $\Delta\nu_{as/s}$ value and the shift of $\nu_{as/s}(CO_3^{2-})$ to 1521 cm^{-1} measured at the samples prepared in the presence of 0.1 mM UO_2^{2+} suggest a bidentate coordination of carbonate ligands to U(VI) adsorbed onto the ferrihydrite surface (Fig. 8E, right). This sorption species is of minor evidence in the sample of initially 0.012 mM UO_2^{2+}, since only a weak shoulder is found in the SD spectrum (Fig. 8C, right). However, the SD spectrum of this sample shows that the $\nu_{as/s}(CO_3^{2-})$ mode shifted to 1488 cm^{-1} ($\Delta\nu_{as/s} \sim 127$ cm^{-1}). This shift may result from electrostatic effects on the surface caused by the presence of divalent cations, because a similar shift to 1484 cm^{-1} occurred when adding Ca^{2+} instead of UO_2^{2+} ions. This observation suggests that in the SD spectra the band at 1488 cm^{-1}, which was observed at initial concentrations up to 0.05 mM U(VI), may still indicate carbonate sorption to the ferrihydrite surface, or probably outer-sphere complexation of uranylcarbonate ions. Hence, the ATR-FTIR results indicate that the contribution of ternary U(VI) carbonato complexes to U(VI) sorption on ferrihydrite is minor at $[U_{tot}] \leqslant 0.012$ mM.

4.5. Refinement of the U(VI)-ferrihydrite complex

Ternary sorption complexes with sulfate and silicate are not a likely explanation of the experimental data, as has been shown and discussed in the previous sections. Here we discuss further details of the proposed binary sorption complex of U(VI) on ferrihydrite. The ATR-FTIR spectra of these sorption samples exhibit the $\nu_3(UO_2^{2+})$ stretching vibration at 903 cm^{-1}. The assignment of this band to dissolved UO_2^{2+} carbonato or hydroxo complexes can be ruled out because these compounds are known to excite bands at substantially higher wavenumbers (>920 cm^{-1}, Khilla et al., 1986; Liger et al., 1999; Quilès and Burneau, 2000). In addition, none of the measured ATR-FTIR spectra show any vibrational indication of secondary minerals of uranyl hydrous oxides from the schoepite family ($[(UO_2)_8O_2(OH)_{12}](H_2O)_x$, $x \leqslant 12$) in the samples. Similar $\nu_3(UO_2^{2+})$ frequencies have been published for U(VI) sorption on ferrihydrite (902 cm^{-1}; Wazne et al., 2003), on hematite in the presence of carbonate (903 cm^{-1}; Ho and Miller, 1986), and on hematite at pH 5.5–8.2 in the absence of CO_2 (906 cm^{-1}; Lefèvre et al., 2006).

No influence of pH on the frequency and shape of the $\nu_3(UO_2^{2+})$ mode was found within the tested pH range. This is similar to results published by Lefèvre et al. (2006). The frequency of the $\nu_3(UO_2^{2+})$ mode did not alter regardless of the presence or absence of atmospheric CO_2 and HCO_3^- ions during U(VI) adsorption onto ferrihydrite. A linkage of carbonate via the O_{ax} atoms of UO_2^{2+} is expected to induce a shift of the $\nu_3(UO_2^{2+})$ band (Čejka, 1999) and thus can be ruled out here. The $\nu_3(UO_2^{2+})$ band shift to lower frequency as compared to the hydrated uranyl ion in water is solely due to the presence of the Fe(III) oxyhydroxide phase and reflects a distortion of the coordination environment of the uranyl ion as it forms an inner-sphere complex on the surface of the solid phase (Liger et al., 1999). This finding should be kept in mind when discussing the spatial topology of UO_2^{2+} sorbed to $Fe(O,OH)_6$ octahedra as gained from the MCTFA approach.

The spatial orientation of the $[UO_2(H_2O)_5]^{2+}$ complex relative to the edge-shared $Fe(O,OH)_6$ octahedron (Fig. 7D) was determined by the interatomic distances that fit the U—O_{eq} and U—Fe shells. These distances coincide with a slight tilt of the edge-sharing polyhedra which means that in addition to the known U—O_{eq} bridging distance another U—O distance of 2.84–2.88 Å arises between U and the apex (ap) of the $Fe(O,OH)_6$ octahedron. This shell, referred to as U—O_{ap}, could be reproduced in all the measured U L_{III}-edge EXAFS spectra by fitting to the FT peak at $R + \Delta \sim 2.4$ Å (Figs. 5 and 6). Note that this 3-D configuration was found by MCTFA routines applied on EXAFS spectra of two different samples, the simulated mine-water precipitate M2 (Ulrich et al., 2006), and the reference sample S11, where U(VI) sorbed ferrihydrite was prepared at $pCO_2 < 0.2$ Pa.

The 3-D topology of the UO_2^{2+} sorption complex calculated by the MCTFA routine represents a tentative model, because the O_{ax} and O_{ap} atoms approach each other at a physically unrealistic distance of ~1.80 Å. Electrostatic repulsion would cause distortion of the polyhedra. Bending of the O=U=O axis rarely obtains angles smaller than 175° (Burns et al., 1997). Out-of-plane coordination of water molecules should weaken the U—O_{ax} bonds and lengthen them. In fact, the measured U—O_{ax} bond distance of 1.80–1.81 Å is substantially larger than the U—O_{ax} bond distance of 1.76 Å of aqueous species such as $[UO_2(H_2O)_5]^{2+}$ (Sémon et al., 2001). According to Kannappan et al. (2004), the origin of an enlarged U—O_{ax} bond length of 1.805 Å is a hydrogen bond O—H $\cdots$ O_{ax} with the length of 2.831 Å. The calculated Fe—O distance is in line with an Fe—OH bond at the apex of the Fe octahedron (Combes et al., 1989). Since the pentahydrated uranyl complex is known to be relatively rigid, a structural relaxation of the ferrihydrite surface was assumed. The fit data do not match a binding structure of UO_2^{2+} to tetrahedrally coordinated iron at the surface, which thus can be ruled out.

The proposed interaction of O_{ax} and O_{ap} may explain the frequency shift of the $\nu_3(UO_2^{2+})$ mode toward lower wavenumbers upon formation of an U(VI)-Fe sorption complex on Fe oxyhydroxides. Further investigation on the structural changes during surface sorption and on the tentative surface complex stabilization by hydrogen bonding is needed, for example quantum chemical methods.

4.6. Geochemical significance

Uranium(VI) is commonly regarded as highly mobile in natural waters. This mobility of U(VI) is primarily attributed to the formation of soluble, relatively stable uranylcarbonato complexes or calcium-uranylcarbonato complexes in the neutral and alkaline pH region, where other heavy metals tend to precipitate. However, there is a pH range where up to 100% of the U(VI) can be attached to Fe-rich colloids by adsorption (cf. Fig. 2). Iron-rich mine-water precipitates are unstable ferrihydrite colloids that tend to aggregate due to their low zeta potential. These aggregating ferrihydrite colloids are able to immobilize U(VI) by the formation of coatings and crusts on the mine rocks. A question of substantial importance is whether this uranium immobilization is irreversible, or can the uranium be released again from the deposits. Furthermore, kinetics of such a release reaction has to be considered. This question is closely related to the type of U(VI) binding to the Fe-rich colloids and colloid aggregates. This study demonstrates that the adsorption of U(VI) onto Fe-rich colloids is not prevented by carbonate at a concentration <0.68 mM. The carbonate can even be involved in this adsorption process. Our spectroscopic investigations show that, depending on the concentrations of U(VI) and carbonate, the type of surface complexes may change from binary uranyl-ferrihydrite to ternary carbonato-uranyl-ferrihydrite complexes. It is to be expected that these different binding mechanisms influence the U(VI) retention at the macroscopic level. However, further research is required to quantitatively relate these molecular structures to the overall behavior of U(VI) in geochemical scenarios.

5. Conclusions

This study investigated the fate of uranium during the simulated flooding of a uranium mine, by characterizing the forming precipitates and the uptake mechanisms of U(VI) by these precipitates. The following conclusions can be drawn by employing both macroscopic and molecular (spectroscopic) methods:

1. The major precipitate forming in the mine water is colloidal ferrihydrite, which rapidly agglomerates. These aggregates remove U(VI) from solution by sorption processes, and not by surface precipitation or structural incorporation.
2. In the absence of dissolved carbonate, a mononuclear inner-sphere, edge-sharing complex forms. By employing a novel EXAFS data evaluation method, MCTFA, we could for the first time ascertain a 3-D binding configuration, which consistently explains the EXAFS data without invoking a ternary carbonato complex. This configuration suggests a slightly tilted position of the adsorbed UO_2^{2+} unit relative to the edge-sharing $Fe(O,OH)_6$ octahedra. In addition to five U—O_{eq} distances attributed to three coordinated water molecules of the hydration sphere and to the bidentate linkage of UO_2^{2+} to the ferrihydrite surface, a slightly longer U—O distance of $\sim 2.86 \pm 0.02$ Å can be explained by an O-atom at the apex of the coordinated $Fe(O,OH)_6$ octahedron. The proposed configuration is a tentative model which needs to be confirmed by complementary methods.
3. In the presence of dissolved carbonate at a pH $\sim$ 8.0, the backscattering contribution at $\sim$4.3 Å can be assigned to a distal carbonate O-atom, supporting an involvement of ternary U(VI) carbonate complexes in U(VI) surface sorption. The occurrence of these complexes was also confirmed by ATR-FTIR.
4. However, at weakly acidic conditions (pH 5–6) in equilibrium with atmospheric CO_2, U(VI) sorption on ferrihydrite is dominated by the binary complex species $\equiv Fe(O)_2{=}UO_2$, whereas ternary U(VI) carbonato surface complexes are of minor relevance.
5. Sulfate and silicate also present in the mine water had no detectable influence on U(VI) surface complexation.

Acknowledgments

The authors kindly acknowledge field sampling support by the WISMUT company. We are grateful to Stephan Weiß, Christine Fröhlich, Ursula Schaefer, Carola Eckardt, Kerstin Muschter (all Institute of Radiochemistry, FZR), Christoph Hennig and Harald Funke (Institute of Radiochemistry, FZR, and Rossendorf Beamline at ESRF) for laboratory work and analytics. Andrea Scholz, Elfi Christalle, and Helfried Reuther (Institute of Ion Beam Physics and Materials Research, FZR) kindly carried out X-ray diffraction, SEM, and Mössbauer spectroscopy. Financial support came from the German Research Foundation (DFG) under contract No. ZA 238/2-1/2. We thank James Noel for linguistic help and Donald L. Sparks and three anonymous reviewers for helpful comments.

Associate editor: Donald L. Sparks

References

Allard, T., Ildefonse, P., Beaucaire, C., Calas, G., 1999. Structural chemistry of uranium associated with Si, Al, Fe gels in a granitic uranium mine. *Chem. Geol.* **158**, 81–103.

Allen, P.G., Bucher, J.J., Shuh, D.K., Edelstein, N.M., Reich, T., 1997. Investigation of aquo and chloro complexes of UO_2^{2+}, $N_pO_2^{+}$, Np^{4+}, and Pu^{3+} by X-ray absorption fine structure spectroscopy. *Inorg. Chem.* **36** (21), 4676–4683.

Amayri, S., Arnold, T., Reich, T., Foerstendorf, H., Geipel, G., Bernhard, B., Massanek, A., 2004. Spectroscopic characterization of the uranium carbonate andersonite $Na_2Ca[UO_2(CO_3)_3]$. $6H_2O$. *Environ. Sci. Technol.* **38**, 6032–6036.

Ankudinov, A.L., Ravel, B., Rehr, J.J., Conradson, S.D., 1998. Real-space multiple-scattering calculation and interpretation of X-ray-absorption near-edge structure. *Phys. Rev. B* **58** (12), 7565–7576.

Bargar, J.R., Reitmeyer, R., Davis, J.A., 1999. Spectroscopic confirmation of uranium(VI)-carbonato adsorption complexes on hematite. *Environ. Sci. Technol.* **33**, 2481–2484.

Bargar, J.R., Reitmeyer, R., Lenhart, J.J., Davis, J.A., 2000. Characterization of U(VI)-carbonato ternary complexes on hematite: EXAFS and electrophoretic mobility measurements. *Geochim. Cosmochim. Acta* **64**, 2737–2749.

Bargar, J.R., Kubicki, J.D., Reitmeyer, R., Davis, J.A., 2005. ATR-FTIR spectroscopic characterization of coexisting carbonate surface complexes on hematite. *Geochim. Cosmochim. Acta* **69**, 1527–1542.

Beleites, M., 1992. *Altlast Wismut*. Brandes & Apsel, Frankfurt (Main), 97 pp..

Bernhard, G., Geipel, G., Brendler, V., Nitsche, H., 1996. Speciation of uranium in seepage waters of a mine tailing pile studied by Time-Resolved Laser-Induced Fluorescence Spectroscopy (TRLFS). *Radiochim. Acta* **74**, 87–91.

Bernhard, G., Geipel, G., Brendler, V., Nitsche, H., 1998. Uranium speciation in waters of different uranium mining areas. *J. Alloys Compd.* **271–273**, 201–205.

Bernhard, G., Geipel, G., Reich, T., Brendler, V., Amayri, S., Nitsche, H., 2001. Uranyl(VI) carbonate complex formation: validation of the $Ca_2UO_2(CO_3)_3(aq)$ species. *Radiochim. Acta* **89**, 511–518.

Blake, R.L., Hessevick, R.E., Zoltai, T., Finger, L.W., 1966. Refinement of the hematite structure. *Am. Mineral.* **51**, 123–129.

Blatov, V.A., Serezhkina, L.B., Serezhkin, V.N., 1990. Crystal structure of $UO_2SO_4 2CH_3CON(CH_3)_2$. *Zh. Strukturnoy Khim.* **31**, 131–133.

Burns, P.C., Ewing, R.C., Hawthorne, F.C., 1997. The crystal chemistry of hexavalent uranium: polyhedral geometries, bond-valence parameters, and polymerization of polyhedra. *Can. Mineral.* **35**, 1551–1570.

Catalano, J.G., Brown Jr., G.E., 2004. Analysis of uranyl-bearing phases by EXAFS spectroscopy: interferences, multiple scattering, accuracy of structural parameters, and spectral differences. *Am. Mineral.* **89**, 1004–1021.

Čejka, J., 1999. Infrared spectroscopy and thermal analysis of the uranyl minerals. In: Burns, P.C., Finch, R. (Eds.), *Uranium: Mineralogy, Geochemistry and the Environment*, *Rev. Mineral.*, vol. 38. Mineralogical Society of America, Washington, DC, pp. 521–622.

Combes, J.M., Manceau, A., Calas, G., Bottero, J.Y., 1989. Formation of ferric oxides from aqueous solutions: a polyhedral approach by X-ray absorption spectroscopy: I. Hydrolysis and formation of ferric gels. *Geochim. Cosmochim. Acta* **53**, 583–594.

Combes, J.M., Manceau, A., Calas, G., 1990. Formation of ferric oxides from aqueous solutions: a polyhedral approach by X-ray absorption spectroscopy: II. Hematite formation from ferric gels. *Geochim. Cosmochim. Acta* **54**, 1083–1091.

Conradson, S.D., 1998. Application of X-ray absorption fine structure spectroscopy to materials and environmental science. *Appl. Spectrosc.* **52**, 252A–279A.

de Jong, W.A., Aprà, E., Windus, T.L., Nichols, J.A., Harrison, R.J., Gutowski, K.E., Dixon, D.A., 2005. Complexation of the carbonate, nitrate, and acetate anions with the uranyl dication: density functional studies with relativistic effective core potentials. *J. Phys. Chem. A* **109** (50), 11568–11577.

Dent, A.J., Ramsay, D.F., Swanton, S.W., 1992. An EXAFS study of uranyl ion in solution and sorbed onto silica and montmorillonite clay colloids. *J. Coll. Interface Sci.* **150**, 45–60.

DIN 38406-E1-1. German standard methods for the examination of water, waste water and sludge. DIN Deutsches Institut fuer Normung e.V., Beuth, Berlin.

Dodge, C.J., Francis, A.J., Gillow, J.B., Halada, G.P., Eng, C., Clayton, C.R., 2002. Association of uranium with iron oxides typically formed on corroding steel surfaces. *Environ. Sci. Technol.* **36**, 3504–3511.

Doelsch, E., Masion, A., Rose, J., Stone, W.E.E., Bottero, J.Y., Bertsch, P.M., 2003. Chemistry and structure of colloids obtained by hydrolysis of Fe(III) in the presence of SiO_4 ligands. *Colloids Surf. A: Physicochem. Eng. Aspects* **217**, 121–128.

Drits, V.A., Sakharov, B.A., Manceau, A., 1993a. Structure of feroxyhyte as determined by simulation of X-ray diffraction curves. *Clay Miner.* **28**, 209–222.

Drits, V.A., Sakharov, B.A., Salyn, A.L., Manceau, A., 1993b. Structural model for ferrihydrite. *Clay Miner.* **28**, 185–207.

Duff, M.C., Coughlin, J.U., Hunter, D.B., 2002. Uranium co-precipitation with iron oxide minerals. *Geochim. Cosmochim. Acta* **66**, 3533–3547.

Feitknecht, W., Giovanoli, R., Michaelis, W., Müller, M., 1973. Über die Hydrolyse von Eisen(III) Salzlösungen. I. Die Hydrolyse der Lösungen von Eisen(III)chlorid. *Helv. Chim. Acta* **56**, 2847–2856.

George, G.N., Pickering, I.J., 2000. *EXAFSPAK. A Suite of Computer Programs for Analysis of X-ray Absorption Spectra*. Stanford Synchrotron Radiation Laboratory, Menlo Park, CA.

Gerth, J., 1990. Unit-cell dimensions of pure and trace metal-associated goethites. *Geochim. Cosmochim. Acta* **54**, 363–371.

Grenthe, I., Fuger, J., Lemire, R.J., Muller, A.B., Nguyen-Trung, C., Wanner, H., 1992. *Chemical Thermodynamics of Uranium*. Elsevier, Amsterdam.

Hennig, C., Reich, T., Dähn, R., Scheidegger, A.M., 2002. Structure of uranium sorption complexes at montmorillonite edge sites. *Radiochim. Acta* **90**, 653–657.

Hennig, C., Tutschku, J., Rossberg, A., Bernhard, G., Scheinost, A., 2005. Comparative EXAFS investigation of uranium(VI) and -(IV) aquo chloro complexes in solution using a newly developed spectroelectrochemical cell. *Inorg. Chem.* **44**, 6655–6661.

Ho, C.H., Miller, N.H., 1986. Adsorption of uranyl species from bicarbonate solution onto hematite particles. *J. Colloid Interface Sci.* **110**, 165–171.

Hsi, C.-K.D., Langmuir, D., 1985. Adsorption of uranyl onto ferric oxyhydroxides: application of the surface complexation site-binding model. *Geochim. Cosmochim. Acta* **49**, 1931–1941.

Hudson, E.A., Allen, P.G., Terminello, L.J., Denecke, M.A., Reich, T., 1996. Polarized X-ray-absorption spectroscopy of the uranyl ion: comparison of experiment and theory. *J. Phys.Rev. B* **54**, 156–165.

Janney, D.E., Cowley, J.M., Buseck, P.R., 2000. Structure of synthetic 2-line ferrihydrite by electron nanodiffraction. *Am. Mineral.* **85**, 1180–1187.

Kannappan, R., Tanase, S., Tooke, D.M., Spek, A.L., Mutikainen, I., Turpeinen, U., Reedijk, J., 2004. Separation of actinides and lanthanides: crystal and molecular structures of N,N'-bis(3,5-dit-butylsalicylidene)-4,5-dimethyl-1,2-phenylenediamine and its uranium complex. *Poyhedron* **23**, 2285–2291.

Khilla, M.A., El-Fekey, E.N., Rofail, N.H., 1986. Infrared absorption study of uranium trioxide phases. *Radiochim. Acta* **40**, 185–190.

Kimball, B.A., Callender, E., Axtmann, E.V., 1995. Effects of colloids on metal transport in a river receiving acid mine drainage, upper Arkansas River, Colorado, USA. *Appl. Geochem.* **10**, 285–306.

Langmuir, D., 1978. Uranium solution-mineral equilibria at low temperatures with applications to sedimentary ore deposits. *Geochim. Cosmochim. Acta* **42**, 547–569.

Lee, G., Bigham, J.M., Faure, G., 2002. Removal of trace metals by coprecipitation with Fe, Al and Mn from natural waters contaminated with acid mine drainage in the Ducktown Mining District, Tennessee. *Appl. Geochem.* **17**, 569–581.

Lefèvre, G., 2004. In situ Fourier-transform infrared spectroscopy studies of inorganic ions adsorption on metal oxides and hydroxides. *Adv. Colloid Interface Sci.* **107**, 109–123.

Lefèvre, G., Noinville, S., Fédoroff, M., 2006. Study of uranyl sorption onto hematite by in situ attenuated total reflection – infrared spectroscopy. *J. Colloid Interface Sci.* **296**, 608–613.

Li, G.G., Bridges, F., Booth, C.H., 1995. X-ray absorption fine-structure standards–a comparison of experiment and theory. *Physical Review B* **52**, 6332–6348.

Liger, E., Charlet, L., Van Cappellen, P., 1999. Surface catalysis of uranium(VI) reduction by iron(II). *Geochim. Cosmochim. Acta* **63**, 2939–2955.

Majzlan, J., Myneni, S.C.B., 2005. Speciation of iron and sulfate in acid waters: aqueous clusters to mineral precipitates. *Environ. Sci. Technol.* **39**, 188–194.

Manceau, A., Combes, J.M., 1988. Structure of Mn and Fe oxides and oxihydroxides: a topological approach by EXAFS. *Phys. Chem. Minerals* **15**, 283–295.

Manceau, A., Drits, V.A., 1993. Local structure of ferrihydrite and feroxyhite by EXAFS spectroscopy. *Clay Miner.* **28**, 165–184.

Manceau, A., Schlegel, M.L., Musso, M., Sole, V.A., Gauthier, C., Petit, P.E., Trolard, F., 2000. Crystal chemistry of trace elements in natural and synthetic goethite. *Geochim. Cosmochim. Acta* **64** (18), 3643–3661.

Moll, H., Geipel, G., Brendler, V., Bernhard, G., Nitsche, H., 1998. Interaction of uranium(VI) with silicic acid in aqueous solutions studied by time-resolved laser-induced fluorescence spectroscopy (TRLFS). *J. Alloys Compd.* **271–273**, 765–768.

Moll, H., Reich, T., Hennig, C., Rossberg, A., Szabo, Z., Grenthe, I., 2000. Solution coordination chemistry of uranium in the binary UO_2^{2+}–SO_4^{2-} and the ternary UO_2^{2+}–SO_4^{2-}–OH^- system. *Radiochim. Acta* **88**, 559–566.

Moyes, L.N., Parkman, R.H., Charnock, J.M., Vaughan, D.J., Livens, F.R., Hughes, C.R., Braithwaite, A., 2000. Uranium uptake from aqueous solution by interaction with goethite, lepidocrocite, muscovite, and mackinawite: an X-ray absorption spectroscopy study. *Environ. Sci. Technol.* **34**, 1062–1068.

Nordstrom, D.K., Alpers, C.N., 1999. Geochemistry of acid mine waters. In: Plumlee, G.S., Logsdon, M.J. (Eds.), *The Environmental Geochemistry of Mineral Deposits*, *Rev. Econ. Geol.*, 6, pp. 133–160.

Ostergren, J.D., Trainor, T.P., Bargar, J.R., Brown Jr., G.E., Parks, G.A., 2000. Inorganic ligand effects on Pb(II) sorption to goethite (α-FeOOH). *J. Colloid Interf. Sci.* **225**, 466–482.

Quilès, F., Burneau, A., 2000. Infrared and Raman spectra of uranyl(VI) oxo-hydroxo complexes in acid aqueous solutions: a chemometric study. *Vibrational Spectrosc.* **23**, 231–241.

Redden, G., Bargar, J., Bencheikh-Latmani, R., 2001. Citrate enhanced uranyl adsorption on goethite: an EXAFS analysis. *J. Coll., Interface Sci.* **244**, 211–219.

Reich, T., Moll, H., Arnold, T., Denecke, M.A., Hennig, C., Geipel, G., Bernhard, G., Nitsche, H., Allen, P.G., Bucher, J.J., Edelstein, N.M., Shuh, D.K., 1998. An EXAFS study of uranium(VI) sorption onto silica gel and ferrihydrite. *J. Electron Spectr. Rel. Phen.* **96**, 237–243.

Reich, T., Bernhard, G., Geipel, G., Funke, H., Hennig, C., Rossberg, A., Matz, W., Schell, N., Nitsche, H., 2000. The Rossendorf Beam Line ROBL – a dedicated experimental station for XAFS measurements of actinides and other radionuclides. *Radiochim. Acta* **88**, 633–637.

Ressler, T., 1998. WinXAS: a program for X-ray absorption spectroscopy data analysis under MS-Windows. *J. Synchrotron Rad.* **5**, 118–122.

Rose, J., Manceau, A., Masion, A., Bottero, J.-Y., 1997. Structure and mechanisms of formation of $FeOOH(NO_3)$ oligomers in the early stage of hydrolysis. *Langmuir* **13**, 3240–3246.

Rossberg, A., Scheinost, A.C., 2005a. Linking Monte Carlo simulation and target transformation factor analysis: a novel tool for the EXAFS analysis of mixtures. *Phys. Scripta* **T115**, 912–914.

Rossberg, A., Scheinost, A.C., 2005b. Three-dimensional modeling of EXAFS spectral mixtures by combining Monte Carlo Simulations and Target Transformation Factor Analysis. *Anal. Bioanal. Chem.* **383**, 56–66.

Scheinost, A.C., Stanjek, H., Schulze, D.G., Gasser, U., Sparks, D.L., 2001a. Structural environment and oxidation state of Mn in goethite–groutite solid-solutions. *Am. Mineral.* **86** (1–2), 139–146.

Scheinost, A.C., Abend, S., Pandya, K.I., Sparks, D.L., 2001b. Kinetic controls on Cu and Pb sorption by ferrihydrite. *Environ. Sci. Technol.* **35** (6), 1090–1096.

Schwertmann, U., Pfab, G., 1996. Structural vanadium and chromium in lateritic iron oxides: genetic implications. *Geochim. Cosmochim. Acta* **60** (21), 4279–4283.

Schwertmann, U., Friedl, J., Stanjek, H., 1999. From Fe(III) ions to ferrihydrite and then to hematite. *J. Colloid Interface Sci.* **209**, 215–223.

Sémon, L., Boehme, C., Billard, I., Hennig, C., Lützenkirchen, K., Reich, T., Rossberg, A., Rossini, I., Wipff, G., 2001. Do perchlorate and triflate anions bind to the uranyl cation in an acidic aqueous medium? A combined EXAFS and quantum mechanical investigation. *ChemPhysChem* **2** (10), 591–598.

Soderholm, L., Skanthakumar, S., Neuefeind, J., 2005. Determination of actinide speciation in solution using high-energy X-ray scattering. *Anal. Bioanal. Chem.* **383**, 48–55.

Su, C., Suarez, D.L., 1997. In situ infrared speciation of adsorbed carbonate on aluminum and iron oxides. *Clays Clay Miner.* **45**, 814–825.

Thompson, H.A., Brown Jr., G.E., Parks, G.A., 1997. XAFS spectroscopic study of uranyl coordination in solids and aqueous solution. *Am. Mineral.* **82**, 483–496.

Ulrich, K.-U., Rossberg, A., Scheinost, A.C., Foerstendorf, H., Zänker, H., Jenk, U., 2006. Speciation of colloid-borne uranium by EXAFS and ATR-IR spectroscopy. In: Merkel, B.J., Hasche-Berger, A. (Eds.), *Uranium in the Environment, Mining Impact and Consequences*. Springer, Berlin, pp. 137–147.

Van Geen, A., Robertson, A.P., Leckie, J.O., 1994. Complexation of carbonate species at the goethite surface: implication for adsorption of metal ions in natural waters. *Geochim. Cosmochim. Acta* **58**, 2073–2086.

Villalobos, M., Leckie, J.O., 2001. Surface complexation modeling and FTIR study of carbonate adsorption on goethite. *J. Colloid Interf. Sci.* **235**, 15–32.

Waite, T.D., Davis, J.A., Payne, T.E., Waychunas, G.A., Xu, N., 1994. Uranium(VI) adsorption to ferrihydrite: application of a surface complexation model. *Geochim. Cosmochim. Acta* **58**, 5465–5478.

Walter, M., Arnold, T., Reich, T., Bernhard, G., 2003. Sorption of uranium(VI) onto ferric oxides in sulfate-rich acid waters. *Environ. Sci. Technol.* **37**, 2898–2904.

Wazne, M., Korfiatis, G.P., Meng, X., 2003. Carbonate effects on hexavalent uranium adsorption by iron oxyhydroxide. *Environ. Sci. Technol.* **37**, 3619–3624.

Webster, J.G., Swedlund, P.J., Webster, K.S., 1998. Trace metal adsorption onto acid mine drainage iron(III) oxy hydroxy sulfate. *Environ. Sci. Technol.* **32**, 1361–1368.

Zänker, H., Richter, W., Hüttig, G., 2003. Scavenging and immobilization of trace contaminants by colloids in the waters of abandoned ore mines. *Colloids Surf. A: Physicochem. Eng. Aspects* **217**, 21–31.